Simplified stress analysis of functionally graded single-lap joints subjected to combined thermal and mechanical loads

Eric Paroissien[1,*], Lucas FM da Silva[2], Frédéric Lachaud[1]

[1] *Institut Clément Ader (ICA), Université de Toulouse, ISAE-SUPAERO, INSA, IMT MINES ALBI, UTIII, CNRS, 3 Rue Caroline Aigle, 31400 Toulouse, France*

[2] *Department of Mechanical Engineering, Faculty of Engineering, University of Porto, Portugal*

*To whom correspondence should be addressed: Tel. +33561338438, E-mail: eric.paroissien@isae-supaero.fr

Abstract – Functionally graded adhesive (FGA) joints involve a continuous variation of the adhesive properties along the overlap allowing for the homogenization of the stress distribution and load transfer, in order to increase the joint strength. The use of FGA joints made of dissimilar adherends under combined mechanical and thermal loads could then be an attractive solution. This paper aims at presenting a 1D-bar and a 1D-beam simplified stress analyses of such multimaterial joints, in order to predict the adhesive stress distribution along the overlap, as a function of the adhesive graduation. The graduation of the adhesive properties leads to differential equations which coefficients can vary the overlap length. For the 1D-bar analyses, two different resolution schemes are employed. The first one makes use of Taylor expansion power series (TEPS) as already published under pure mechanical load. The second one is based on the macro-element (ME) technique. For the 1D-beam analysis, the solution is only based on the ME technique. A comparative study against balanced and

unbalanced joint configurations under pure mechanical and/or thermal loads involving constant or graduated adhesive properties are provided to assess the presented stress analyses. The mathematical description of the analyses is provided.

Key words*: functionally graded adhesive; single-lap bonded joint; stress analysis; macro-element; thermoelasticity; dissimilar adherend.*

NOMENCLATURE AND UNITS

A_j extensional stiffness (N) of adherend j

B_j extensional and bending coupling stiffness (N.mm) of adherend j

D_j bending stiffness (N.mm^2) of adherend j

E_a adhesive peel modulus (MPa)

$E_{a,min}$ adhesive shear modulus (MPa)

$E_{a,max}$ adhesive shear modulus (MPa)

E_j adherend Young's modulus (MPa) of adherend j

F magnitude of applied force (N)

F_e element nodal force vector

$F_{e,therm}$ element nodal force vector equivalent to thermal load

G_a adhesive shear modulus (MPa)

$G_{a,max}$ maximal adhesive shear modulus (MPa)

$G_{a,min}$ minimal adhesive shear modulus (MPa)

K_{BBa} elementary stiffness matrix of a bonded-bars element

K_{BBe} elementary stiffness matrix of a bonded-beams element

$K_{bar,j}$ elementary stiffness matrix of a bar for the adherend j

L length (mm) of bonded overlap

M_e element matrix linking the element nodal displacement to the constant integration

vector

M_j bending moment (N.mm) in adherend j around the z direction

M_e element matrix linking the element nodal force to the constant integration vector

$M_j^{\Delta T}$ thermal bending moment (N.mm) in adherend j around the z direction

N_j normal force (N) in adherend j in the x direction

$N_j^{\Delta T}$ thermal normal force (N) in adherend j in the x direction

3

S	adhesive peel stress (MPa)
T	adhesive shear stress (MPa)
T_{max}	maximal adhesive shear stress (MPa)
U_e	element nodal displacement vector
V_j	shear force (N) in adherend j in the y direction
b	width (mm) of the adherends
c	half-length (mm) of bonded overlap
e_a	thickness (mm) of the adhesive layer
h_j	half thickness (mm) of adherend j
k_I	adhesive elastic stiffness (MPa/mm) in peel
k_{II}	adhesive elastic stiffness (MPa/mm) in shear
n_max	order of truncation
n_ME	number of macro-elements
p	power of the graduation law
u_j	displacement (mm) of adherend j in the x direction
v_j	displacement (mm) of adherend j in the y direction
Δ	overlap length (mm) of a macro-element
Δ_T	variation of temperature (K)
Δu	slipping displacement (mm)
Δ_j	characteristic parameter ($N^2.mm^2$) of adherend j
α_j	coefficient of thermal expansion (K^{-1}) of adherend j
θ_j	bending angle (rad) of the adherend j around the z direction
χ_A	adherend stiffness unbalance parameter (-)
χ_α	adherend thermal unbalance parameter (-)
(X,Y,Z)	element reference system of axes

(x,y,z) global reference system of axes

BBa   Bonded-bars

BBE   Bonded-beams

CTE   coefficient of thermal expansion

FE   Finite Element

FGA   functionally graded adhesive

GM   general model

ISLM   improved shear-lap model

JE   joint element

ME   macro-element

ODE   ordinary differential equation

TC   test case

TEPS   Taylor expansion in power series

1. Introduction

In the frame of structural design, the proper choice of joining technology is decisive for the integrity of the manufactured structure. Mechanical fastening, such as riveting or screwing, appears to be a reliable solution for the designers. Nevertheless, alone or in combination with mechanical fastening, the adhesive bonding technology may offer significantly improved mechanical performance in terms of stiffness, static strength and fatigue strength [1-3]. Indeed, unlike the discrete load transfer of mechanical fasteners, the load transfer between structural bonded components is continuous all along the overlap. This higher level of mechanical performance allows for lighter joints. In other words, adhesive bonding offers the possibility to reduce the structural mass while ensuring the mechanical strength. The optimization of the strength-to-weight ratio is a challenge for several industrial sectors, such as aerospace, automotive, rail or naval transport industries.

Nevertheless, stress gradients at both overlap ends appear in bonded joints, due to the relative deformation of the adhesive layer with regards to the adherends. It leads to a load transfer restricted on a small length at the overlap ends. In order to increase the load capability of bonded joints, the reduction of adhesive peak stresses is wanted. The specimen design for the thick adherend shear test [4] leads to both a homogenization of the adhesive shear stress and a drastic reduction the adhesive peel stress, all the more when care is taken to reduce the edge effects [5]. Another approach is to make the material and/or geometrical properties of the adherends and/or the adhesive layer vary along the overlap. Several design solutions have been published [3]. For example, a solution is the tapering of adherends at overlap ends, which allows for a progressive increase of the neutral line lag and a reduction of adhesive peel stress [6-7]. A more local solution is the rounding of adherend corner associated with adhesive spew fillets [8-9]. The mixed adhesive solution which is a rough version of a graded joint consists in the use of various different adhesives along the overlap to increase the joint

strength [10-13]. In recent past years, functionally graded adhesive (FGA) have been more and more considered [14-15]. FGA joints involve a continuous variation of the adhesive properties along the overlap allowing for the homogenization of the stress distribution and load transfer. When dissimilar adherends have to be bonded, the adhesive stress distribution is asymmetrical, so that one of the overlap ends is overstressed. Moreover, this overstressing is magnified under thermal loads due to the mismatch in coefficient of thermal expansion (CTE) of adherends. The capability of a local graduation of the adhesive stiffness is a promising solution to optimize the strength of multimaterial joints under severe loads, such as combined thermal and mechanical. This situation occurs very often in multi-material structures found in the transport industry. That is why the development of dedicated stress analyses to predict the stress distribution is fundamental. The Finite Element (FE) method is able to address the stress analysis of FGA joints [12,14]. Nevertheless, since analyses based on FE models are computationally costly, it would be profitable both to restrict them to refined analyses and to develop simplified approaches, enabling extensive parametric studies and optimization processes. Moreover, numerous simplified stress analyses of bonded joints are available and provide accurate predictions [16-18]. In 2014, Carbas et al. published a first analytical approach for 1D-bar stress analysis of FGA joints [19]. This stress analysis is based on the shear-lag approach by Volkersen [20] associated with a resolution scheme making use of Taylor expansion in power series (TEPS) to solve the involved differential equations. This stress analysis is restricted to half of the overlap length of balanced joints with a linear graduation of the adhesive shear modulus. Stein et al. presented a 1D-bar analysis using TEPS resolution able to address unbalanced bonded joints under any adhesive properties graduations [21-22]. This analysis is called by the authors Improved Shear Lag Model (ISLM). Moreover, Stein et al. provided a sandwich-type analysis using TEPS resolution, taking into accounts both in-plane and out-of-plane load, termed General Model (GM). The sandwich-type

7

analysis concept comes from the analysis methodology by Goland and Reissner [23] who provided the first closed-form solution for the adhesive stress distribution for simply supported balanced joint made of adherends undergoing cylindrically bending. Goland and Reissner took into account the geometrical non linearity due to the lag of neutral line to assess the bending moment at both overlap ends through a bending moment factor. This methodology was then employed by other researchers to improve the initial model [24-32] leading to various forms of the bending moment factor [33]. In 2017, Stapleton et al. used a joint element (JE) for the stress analysis of FGA joints under various geometrical configurations, including in-plane and out-of-plane load as well as non-linear material behavior [34]. A JE is a 4-nodes brick element allowing for the modelling of two bonded adherends [34-35]. Over a similar period of time, the first and third authors of the present papers and co-workers have been working on the development of the macro-element (ME) technique for the simplified stress analysis of bonded, bolted and hybrid (bonded/bolted) joints [36-43]. Dedicated 4-nodes Bonded-bars (BBa) and Bonded-beams (BBe) have been formulated. As for the JE model, only one BBa or BBe, depending on the chosen kinematics, is sufficient to be representative for an entire bonded overlap in the frame of a linear elastic analysis (see Figure 1). When the geometrical or material properties of the adherends or the adhesive layer vary along the overlap a mesh is necessary along the overlap length direction only. The ME technique is inspired by the FE method and differs in the sense that the interpolation functions are not assumed. Indeed, they take the shape of solutions of the governing ordinary differential equations (ODEs) system, coming from the constitutive equations of the adhesive and adherends and from the local equilibrium equations, related to the simplifying hypotheses. The main work is thus the formulation of the elementary stiffness matrix of the ME. Once the stiffness matrix of the complete structure is assembled from the elementary matrices and the boundary conditions are applied, the minimization of the

potential energy provides the solution, in terms of adhesive stress distributions along the overlap, internal forces and displacements in the adherends. The ME technique can be regarded as mathematical procedure allowing for the resolution of the system of ODE, under a less restricted application field of simplifying hypotheses, in terms of geometry, material behaviours, kinematics, boundary conditions and loads.

Stress analyses of bonded joints under thermal loads can be found in the literature linked to the aerospace [44] or to the emergence of the industry of electronic packaging [45-48]. However, to the best knowledge of authors, there is not any published stress analyses of FGA joints under thermal load. The present paper aims at presenting simplified stress analysis of FGA single-lap joints under combined mechanical and thermal loads. Under the 1D-bar kinematics, the resolution scheme by TEPS and by ME is used. As the 1D-bar TEPS and ME analyses provide the same predictions, the resolution scheme by ME under the 1D-beam kinematics is employed only. Indeed, the ME technique offers the possibility to extend the application field to analyses involving nonlinear material behaviors, various geometries and various applied boundary conditions [39-43]. The developed stress analyses are then assessed against reference stress analyses for bonded and FGA joints on several test cases. The three stress analyses presented need dedicated computer codes, which are provided as supplementary materials with the present papers. These codes run on the MATLAB commercial software. Moreover, for the comfort of readers, this paper provides the useful mathematical steps, even if some elements have eventually been published elsewhere.
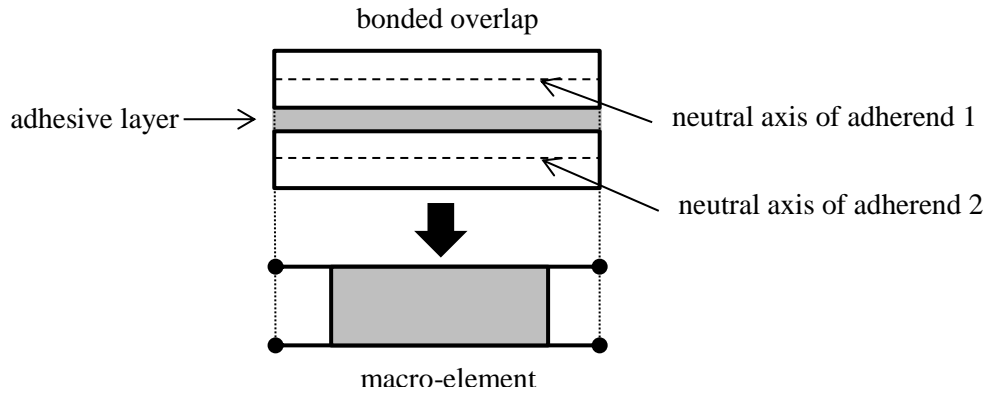
Figure 1. Modelling of a bonded overlap by a macro-element.

2. Description of simplified stress analyses of FGA single-lap joints

2.1. Under 1D-bar kinematics

2.1.1 Hypotheses

The following hypotheses are taken (i) the adherends are linear elastic materials simulated as bars, (ii) the adhesive layer is simulated by an infinite number of linear elastic shear springs linking both adherends, and (iii) the shape of graduation of the adhesive layer shear modulus is considered. As a result, it is supposed that all the adhesive stress components vanish except the in-plane shear. The case of a single-lap joint subjected to combined mechanical and thermal loads is considered. The geometrical parametrization is provided in Figure 2. The subscript 1 (2) refers to the upper (lower) adherend. The origin of the global reference system is taken at the centre of the overlap, with the x-axis along the overlap length direction, the only axis according to which displacements u are possible. The joint is submitted to an uniform variation of temperature Δ_T, to a tensile force F at one extremity and is fixed at the other one. The stress analysis is conducted in force but could similarly be made in tensile flow F/b.
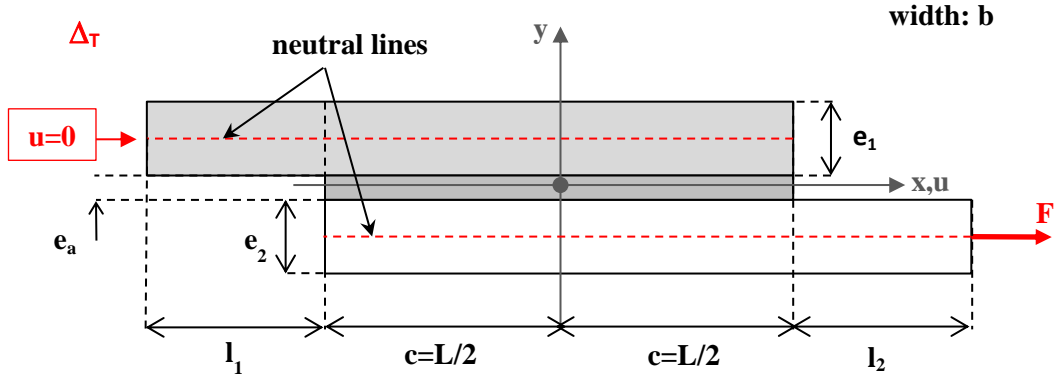
Figure 2. Geometrical parametrization of the single-lap joint, boundary conditions and applied loads (1D-bar analysis).

2.1.2 Governing equations

The local equilibrium of both adherends (see Figure 3) provides the following equations:

$$\frac{dN_j}{bdx} = (-1)^j T(x), j = 1,2 \tag{1}$$

where b is the overlap width, N_j the normal force in the adherend j and T the adhesive shear stress.
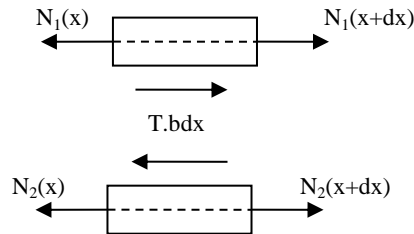

Figure 3. Free body diagram of infinitesimal pieces included between x and $x+dx$ of both adherends in the overlap region. Subscript 1 (2) refers to the upper (lower) adherend.

The total strain is equal to the mechanical strain plus the thermal strain such as:

$$\frac{du_j}{dx} = \frac{N_j}{A_j} + \alpha_j \Delta_T, \ j = 1,2 \tag{2}$$

where α_j is the coefficient of thermal expansion of the adherend j. A_j is the membrane stiffness of the adherend j, given by:

$$A_j = E_j b e_j \tag{3}$$

11

where e_j is the thickness of the adherend j and E_j the Young's modulus of the adherend. The displacement $u_j(x)$ is the normal displacement of points located at the abscissa x on the neutral line of adherend j (see Figure 2).

The constitutive equation for the adhesive layer is provided by:

$$T = G_a \frac{u_2 - u_1}{e_a} = k_{II}\Delta u \tag{4}$$

with:

$$\Delta u = u_2 - u_1 \tag{5}$$

where e_a is the adhesive thickness, G_a the adhesive shear modulus and $k_{II}=G_a/e_a$ the adhesive shear relative stiffness. Δu is the differential displacement of the adherend interface. The stress analyses presented use k_{II} and Δu, so that they can be directly applied when the thickness of the adhesive layer varies along the overlap.

2.1.3 TEPS resolution

The approach using TEPS resolution scheme is firstly used. The differentiation of Eq. (2) with respect to x provides:

$$\frac{d^2 u_j}{dx^2} = \frac{1}{A_j}\frac{dN_j}{dx}, \ j = 1,2 \tag{6}$$

By using the local equilibrium equation Eq. (1) and the adhesive constitutive equation Eq. (4), it comes:

$$\frac{d^2 u_j}{dx^2} = \frac{1}{A_j}(-1)^j bT(x) = \frac{b}{A_j}(-1)^j k_{II}\Delta u, \ j = 1,2 \tag{7}$$

As a result, a second order differential equation in the slipping displacement (relative horizontal displacement of the interface) can be written:

$$\frac{d^2 \Delta u}{dx^2} - \tilde{\eta}^2 k_{II}\Delta u = 0 \tag{8}$$

with:

$$\tilde{\eta}^2 = \frac{1}{e_1 E_1} + \frac{1}{e_2 E_2} = \frac{1+\chi_A}{A'_2} \tag{9}$$

$$\chi_A = \frac{A'_2}{A'_1} = \frac{e_2 E_2}{e_1 E_1} = \frac{A_2}{A_1} \tag{10}$$

A'_j is the membrane stiffness of the adherend j per unit of width. χ_A is representative for the stiffness unbalance of the joint. The differential equation Eq. (8) is relevant to the one obtained by Stein et al. for the ISLM – which does not consider any thermal load – but written in slipping displacement instead of shear strain [22]. A solution is then searched for any x included between $-c$ and c under the shape of TESP:

$$\Delta u(x) = \sum_{n=0}^{\infty} u_n x^n \tag{11}$$

For the series terms to have the same unit as the function approximated, the following variable change is made in the present analysis:

$$\zeta = \frac{x}{c} \tag{12}$$

As result, the solution is searched for any X included between -1 and 1 under the shape:

$$\Delta u(x) = \sum_{n=0}^{\infty} u_n (c\zeta)^n = \sum_{n=0}^{\infty} u_n c^n \zeta^n = \sum_{n=0}^{\infty} U_n \zeta^n \tag{13}$$

with:

$$\forall n, \ U_n = c^n u_n \tag{14}$$

The mth derivative of Δu is then assessed as follows

$$\frac{d^m \Delta u}{dx^m} = \frac{1}{c^m} \frac{d^m \Delta u}{d\zeta^2} = \frac{1}{c^m} \sum_{n=0}^{\infty} \prod_{i=1}^{m} (n+i) \, U_{n+2} \zeta^n \tag{15}$$

The graduation of adhesive properties is then described under the shape of a TESP:

$$k_{II}(\zeta) = \sum_{n=0}^{\infty} K_n \zeta^n = \sum_{n=0}^{\infty} k_n x^n = k_{II}(\zeta) \tag{16}$$

with:

$$\forall n, \ K_n = c^n k_n \tag{17}$$

The expressions for Δu and k_{II} are then replaced in the second order differential equation Eq. (8) leading to:

$$\sum_{n=0}^{\infty} (n+1)(n+2) U_{n+2} \zeta^n - c^2 \tilde{\eta}^2 \sum_{n=0}^{\infty} U_n X^n \sum_{l=0}^{\infty} K_l \zeta^l = 0 \tag{18}$$

13

Equating each term to zero, the following recursive relationship is then obtained:

$$\forall n, \ U_{n+2} = \frac{c^2 \tilde{\eta}^2}{(n+1)(n+2)} \sum_{l=0}^{n} U_l K_{n-l} \tag{19}$$

This recursion relationship is of course similar to the one obtained by Stein et al. [22]. Two boundary conditions have to be applied to be able to determine the terms of the series. In this paper, the values of the normal forces in the lower adherend are used, which reads:

$$N_2(x = -c) = 0 = N_2(X = -1) \tag{20}$$

$$N_2(x = c) = F = N_2(X = 1) \tag{21}$$

A relationship between the sipping displacement and the normal force in the lower adherend is then established as follows. From Eq. (2) and since the sum of the normal force of the upper adherend and that of the lower adherend is equal to F at any position along the overlap, the slipping displacement is written such as:

$$\frac{d\Delta u}{dx} = (1 + \chi_A) \frac{N_2}{A_2} - \chi_A \frac{F}{A_2} + \left(1 - \frac{1}{\chi_\alpha}\right) \alpha_2 \Delta_T \tag{22}$$

where the adherend thermal unbalance is characterized by:

$$\chi_\alpha = \frac{\alpha_2}{\alpha_1} \tag{23}$$

As a result, from the application of boundary conditions in Eq. (20) and Eq. (21), both last required equations are obtained.

$$\sum_{n=0}^{\infty} (n + 1) U_{n+1} = c \frac{F}{A_2} + c \left(1 - \frac{1}{\chi_\alpha}\right) \alpha_2 \Delta_T \tag{24}$$

$$\sum_{n=0}^{\infty} (n + 1)(-1)^n U_{n+1} = -c \chi_A \frac{F}{A_2} + c \left(1 - \frac{1}{\chi_\alpha}\right) \alpha_2 \Delta_T \tag{25}$$

These last equations allow for the introduction of the thermal load in the model. The solution is finally obtained by truncation of the series at an order *n_max*. Equations Eq. (19), Eq. (24) and Eq. (25) allow for the writing of a linear system, the size of which is *(n_max+1)²*, which can be solved using a mathematical programming software such as MATLAB.

2.1.4 ME resolution

Firslty, the elementary stiffness matrix of a BBa element is formulated. The length of the BBa is Δ, on which the material and geometrical properties are supposed constant. The element reference system of axis is denoted (X,Y,Z). The elementary stiffness matrix of the BBa, termed K_{BBa}, describes the interaction between the four nodal forces and the force nodal displacements (see Figure 4), such as:

$$\begin{pmatrix} -N_1(0) \\ -N_2(0) \\ N_1(\Delta) \\ N_2(\Delta) \end{pmatrix} = K_{BBa} \begin{pmatrix} u_1(0) \\ u_2(0) \\ u_1(\Delta) \\ u_2(\Delta) \end{pmatrix} \Leftrightarrow F_e = K_{BBa} U_e \tag{26}$$

where F_e (U_e) is the nodal force (displacement) vector of the BBa element.
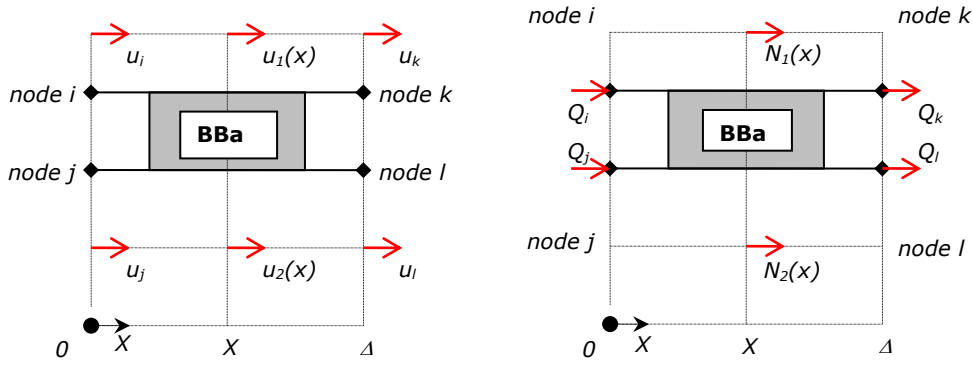
Figure 4. Free body diagram of infinitesimal pieces included between x and $x+dx$ of both adherends in the overlap region. Subscript 1 (2) refers to the upper (lower) adherend.

In the frame of the 1D-bar analysis, the closed-form expressions for each component of K_{BBa} can be obtained [36-37]. Even if the mathematical description has already published under another shape, it provided in Appendix A.

As expected, the obtained stiffness matrix is the same as the one obtained without considering the thermal load. The method to take into account a linear variation of shear stress in the adherend thickness following [28] is described in Appendix D.

Since the material properties of the adhesive vary along the overlap, the approach using the ME technique consists in regularly meshing the overlap with BBa elements with n_ME BBa elements (see Figure 5). Each BBa element has a length $\Delta=L/n\_ME$, on which the material

properties are constant. The actual graduation of the adhesive shear relative stiffness has then to be approximated by a stepped function. In this work, it is supposed that the adhesive shear relative stiffness for the nth BBa is equal to its value at the centre of the BBa. The elementary stiffness matrices of the each BBa can then be assessed. The bars outside the overlap are simulated as bar elements associated with the elementary stiffness matrix $K_{bar,j}$ for adherend j given in Appendix A. From the elementary stiffness matrices, the stiffness matrix of the joint, termed K_s, is then built. The boundary conditions are applied using the classical FE rules. In particular, the thermal load is replaced by an equivalent mechanical one, such that the equivalent nodal force vector provides the same nodal displacement as the thermal load. The potential energy leading to the classical linear system $F_s = K_s U_s$, the size of which is $(2n\_ME+4)^2$, where F_s is the nodal force of the structure and U_s the nodal vector.
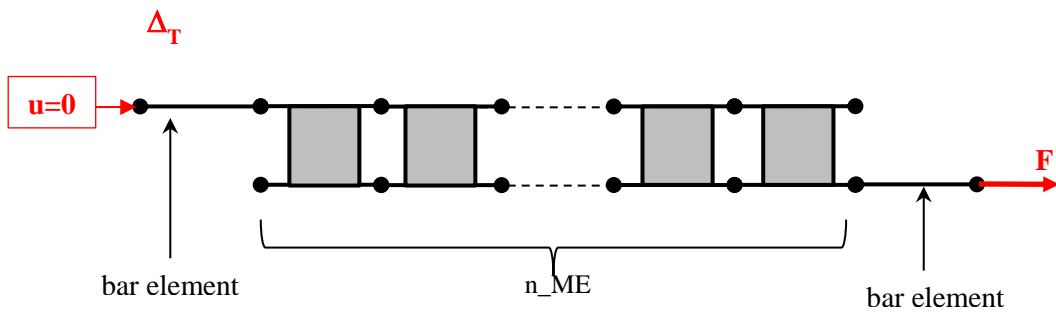
Figure 5. ME model of the FGA single lap joint.

2.2.   *Under 1D-beam kinematics*

2.1.1   *Hypotheses*

The model is based on the following hypotheses: (i) the thickness of the adhesive layer is constant along the overlap, (ii) the adherends are simulated by linear elastic Euler-Bernoulli laminated beams and (iii) the adhesive layer is simulated by an infinite number of elastic shear and transverse springs linking both adherends.

16

Similarly to the 1D-bar analysis, the case of a single-lap joint subjected to combined mechanical and thermal loads is considered, for which the geometrical parametrization is provided in Figure 6. The joint is simply supported at both extremities and submitted to a uniform variation of temperature Δ_T and to a tensile force F. It is indicated that any boundary conditions could be applied when the ME technique is applied, even if simply supported is chosen in this paper. The stress analysis is conducted in force but could similarly be made in tensile flow F/b.
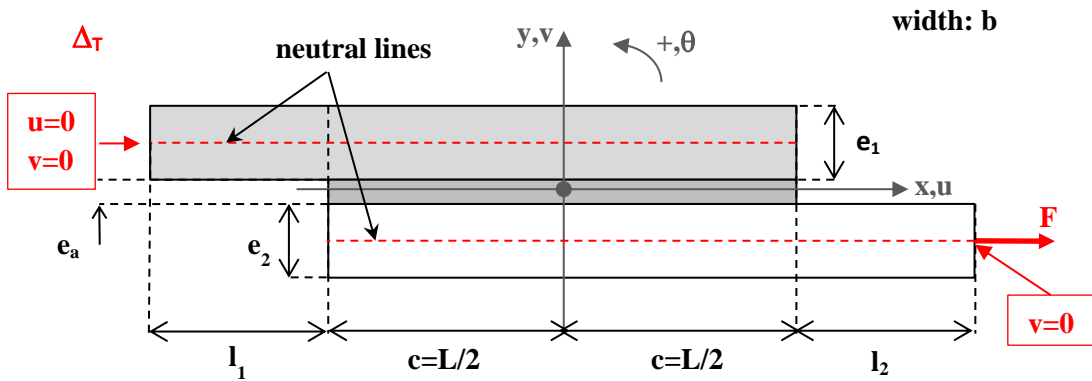
Figure 6. Geometrical parametrization of the single-lap joint, boundary condition and applied loads (1D-beam analysis).

2.2.2 Governing Equation

The local equilibrium selected for the formulation of the presented BBe element is related to the one used by Luo and Tong [31] and allows for a coupling between the in-plane and out-of-plane load. Moreover, the formulation presented can be easily modified to correspond to the Goland and Reissner [23] or to the Hart-Smith [24] local equilibrium.

The local equilibrium of both adherends (see Figure 7) provides the six following equations:

$$\frac{dN_j}{dX} = (-1)^j \cos\theta_j \, bT, \quad j = 1,2 \tag{27}$$

$$\frac{dV_j}{dX} = (-1)^{j+1} bS + (-1)^j \sin\theta_j \, bT, \quad j = 1,2 \tag{28}$$

$$\frac{dM_j}{dX} + V_j + \cos\theta_j \, b\left(h_j + \frac{e_a}{2}\right) T - \sin\theta_j \, N_j = 0, \quad j = 1,2 \tag{29}$$

17

with:

$$h_j = \frac{e_j}{2}, j = 1,2 \tag{30}$$

where V_j is the shear force in the adherend j, M_j the bending moment in the adherend j, θ_j the

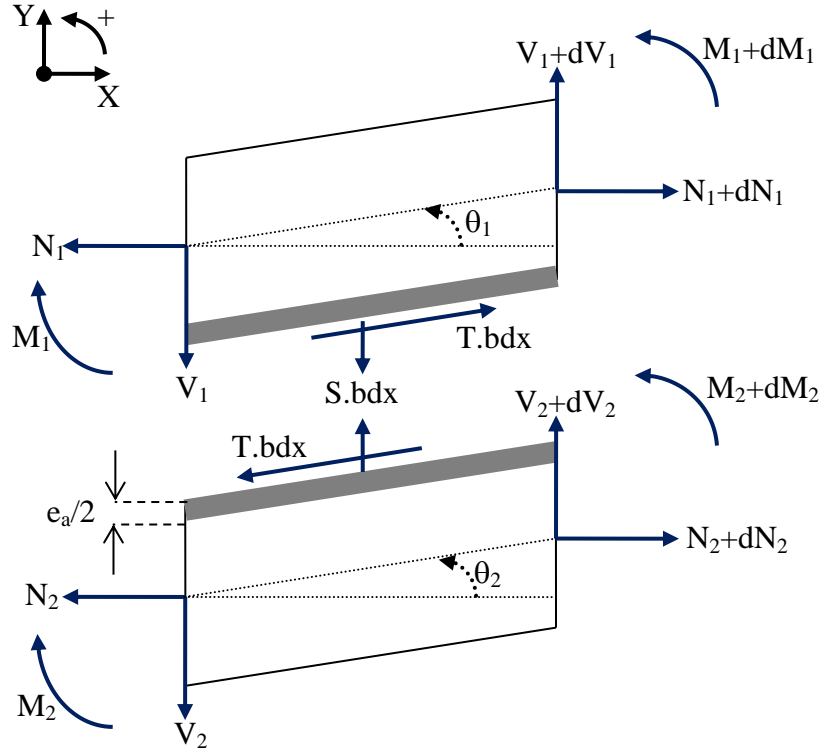bending angle in the adherend j and S is the adhesive peel stress.

Figure 7. Free body diagram of infinitesimal pieces included between x and $x+dx$ of both

adherends in the overlap region. Subscript 1 (2) refers to the upper (lower) adherend.

The constitutive equations can then be written as:

$$N_j = A_j \frac{du_j}{dX} - B_j \frac{d\theta_j}{dX} - N_j^{\Delta_T}, \ j = 1,2 \tag{31}$$

$$M_j = -B_j \frac{du_j}{dX} + D_j \frac{d\theta_j}{dX} + M_j^{\Delta_T}, \ j = 1,2 \tag{32}$$

$$\theta_j = \frac{dv_j}{dX} \tag{33}$$

where (see Appendix A) A_j is the membrane stiffness of adherend j, B_j the coupling

membrane-bending stiffness of adherend j, D_j the bending stiffness of adherend j, $N_j^{\Delta_T}$ the

thermal normal force in the adherend j and $M_j^{\Delta T}$ is the thermal bending moment in the adherend j. In the case of a lay-up characterized by a mirror symmetry, $B_j=0$ and $M_j^{\Delta T} = 0$.

The constitutive equations for the adhesive layer are provided by:

$$S = \frac{E_a}{e_a}[v_1 - v_2] = k_I \Delta v \tag{34}$$

$$T = \frac{G_a}{e_a}[u_2 - h_2\theta_2 - (u_1 + h_1\theta_1)] = k_{II}\Delta u \tag{35}$$

with:

$$\Delta u = u_2 - u_1 - h_2\theta_2 - h_1\theta_1 \tag{36}$$

$$\Delta v = v_1 - v_2 \tag{37}$$

where E_a is the adhesive peel modulus and $k_I=E_a/e_a$ the adhesive peel relative stiffness. Δv is representative of the opening displacement of the adherend interface. Contrary to the 1D-bar analysis, the presented analysis cannot be directly applied when the thickness of the adhesive layer varies along the overlap. Indeed, the variation of the thickness induces a lag of the neutral axis, which has to be taken into account because of the deflection. Nevertheless, it is indicated that the variation of the adhesive thickness could be easily taken into account when using the ME technique.

2.2.3 ME resolution

The resolution scheme follows the same part as for the 1D-bar analysis (see section 2.1.4). The single-lap joint is meshed in BBe elements along the overlap and beam elements for the parts outside the overlap. The boundary conditions, the mechanical and thermal loads are then applied. Similarly to the 1D-bar analysis, the thermal load is applied under the shape of an equivalent nodal force vector given by:

$$F_{th} = \begin{pmatrix} -N_1^{\Delta_T} \\ -N_2^{\Delta_T} \\ N_1^{\Delta_T} \\ N_2^{\Delta_T} \\ 0 \\ 0 \\ 0 \\ 0 \\ M_1^{\Delta_T} \\ M_2^{\Delta_T} \\ -M_1^{\Delta_T} \\ -M_2^{\Delta_T} \end{pmatrix} \tag{38}$$

Contrary to the 1D-bar analysis, it is not possible to simply obtain closed-form expressions for the components of the stiffness matrix of the BBe element. An approach for the formulation of the stiffness matrix of BBe element under Goland and Reissner equilibrium has already been described in detail in previous papers [36-43]. Nevertheless, this approach could be long to set up. In this paper, a new approach is provided for a fast and easy implementation within mathematical software such as MATLAB for example. The present formulation ME has never been published. The element reference system (X,Y,Z) of axes is considered. Following Luo and Tong approach [31], a first approximation is made. The bending angle is supposed very small. The six local equilibrium equations become then:

$$\frac{dN_j}{dX} = (-1)^j bT, \ \ j = 1,2 \tag{39}$$

$$\frac{dV_j}{dX} = (-1)^{j+1} bS + (-1)^j \theta_j bT, \ j = 1,2 \tag{40}$$

$$\frac{dM_j}{dX} + V_j + b\left(h_j + \frac{e_a}{2}\right)T - \theta_j N_j = 0, \ \ j = 1,2 \tag{41}$$

A second approximation is made. It consists in neglecting the product of the adhesive shear stress with the bending angle $T\theta_j \ll 1, \ j = 1,2$. The six local equilibrium equations become then:

$$\frac{dN_j}{dX} = (-1)^j bT, \ \ j = 1,2 \tag{42}$$

$$\frac{dV_j}{dX} = (-1)^{j+1} bS, \quad j = 1,2 \tag{43}$$

$$\frac{dM_j}{dX} + V_j + b\left(h_j + \frac{e_a}{2}\right)T - \theta_j N_j = 0, \quad j = 1,2 \tag{44}$$

Compared to the local equilibrium by Hart-Smith [24] only the bending moment is modified, involving a coupling between normal forces and bending moment. The following quotation is introduced for any functions f:

$$\binom{f_+}{f_-} = \begin{pmatrix} 1 & 1 \\ 1 & -1 \end{pmatrix} \binom{f_1}{f_2} \tag{45}$$

A third and last approximation is made which reads $\frac{N_-}{2}(\theta_1 \mp \theta_2) \ll 1$. Under this approximation and taking into account that the sum of normal forces at any abscissa is equal to the applied force F, a system of twelve first order linear ODEs is obtained:

$$\frac{du_+}{dX} = \frac{1}{2}\left(\frac{D_1}{\Delta_1} + \frac{D_2}{\Delta_2}\right)N_+ + \frac{1}{2}\left(\frac{D_1}{\Delta_1} - \frac{D_2}{\Delta_2}\right)N_- + \frac{1}{2}\left(\frac{B_1}{\Delta_1} + \frac{B_2}{\Delta_2}\right)M_+ + \frac{1}{2}\left(\frac{B_1}{\Delta_1} - \frac{B_2}{\Delta_2}\right)M_- \tag{46}$$

$$\frac{dv_+}{dX} = \theta_+ \tag{47}$$

$$\frac{d\theta_+}{dX} = \frac{1}{2}\left(\frac{B_1}{\Delta_1} + \frac{B_2}{\Delta_2}\right)N_+ + \frac{1}{2}\left(\frac{B_1}{\Delta_1} - \frac{B_2}{\Delta_2}\right)N_- + \frac{1}{2}\left(\frac{A_1}{\Delta_1} + \frac{A_2}{\Delta_2}\right)M_+ + \frac{1}{2}\left(\frac{A_1}{\Delta_1} - \frac{A_2}{\Delta_2}\right)M_- \tag{48}$$

$$\frac{du_-}{dX} = \frac{1}{2}\left(\frac{D_1}{\Delta_1} - \frac{D_2}{\Delta_2}\right)N_+ + \frac{1}{2}\left(\frac{D_1}{\Delta_1} + \frac{D_2}{\Delta_2}\right)N_- + \frac{1}{2}\left(\frac{B_1}{\Delta_1} - \frac{B_2}{\Delta_2}\right)M_+ + \frac{1}{2}\left(\frac{B_1}{\Delta_1} + \frac{B_2}{\Delta_2}\right)M_- \tag{49}$$

$$\frac{dv_-}{dX} = \theta_- \tag{50}$$

$$\frac{d\theta_-}{dX} = \frac{1}{2}\left(\frac{B_1}{\Delta_1} - \frac{B_2}{\Delta_2}\right)N_+ + \frac{1}{2}\left(\frac{B_1}{\Delta_1} + \frac{B_2}{\Delta_2}\right)N_- + \frac{1}{2}\left(\frac{A_1}{\Delta_1} - \frac{A_2}{\Delta_2}\right)M_+ + \frac{1}{2}\left(\frac{A_1}{\Delta_1} + \frac{A_2}{\Delta_2}\right)M_- \tag{51}$$

$$\frac{dN_+}{dX} = 0 \tag{52}$$

$$\frac{dV_+}{dX} = 0 \tag{53}$$

$$\frac{dM_+}{dX} = -V_+ + \frac{G}{e}bh_+.u_- + \left(\frac{G}{2e}b(h_+ + e_a)^2 + \frac{F}{2}\right)\theta_+ + \left(\frac{G}{2e}b(h_+ + e_a)h_-\right)\theta_- \tag{54}$$

$$\frac{dN_-}{dX} = 2k_{II}b.u_- + k_{II}b(h_+ + e_a)\theta_+ + k_{II}bh_-\theta_- \tag{55}$$

$$\frac{dV_-}{dX} = 2k_I b.w_- \tag{56}$$

$$\frac{dM_-}{dX} = -V_- + \frac{G}{e}bh_-.u_- + \left(\frac{G}{2e}b(h_+ + e_a)h_-\right)\theta_+ + \left(\frac{G}{2e}bh_-^2 + \frac{F}{2}\right)\theta_- \tag{57}$$

where $\Delta_j = A_j D_j - B_j B_j \neq 0$. By letting $F=0$, the stress analysis of the sandwich by Hart-Smith is deduced [24]. In addition, by letting $e_a = 0$, it corresponds to the one by Goland and Reissner [23]. This system can be written as $\frac{dV}{dX} = AV$ where A is 12x12 matrix with real constant components and the unknown vector V is such that ${}^tV = (u_1\ u_2\ v_1\ v_2\ \theta_1\ \theta_2\ N_1\ N_2\ V_1\ V_2\ M_1\ M_2)$. But the elementary stiffness matrix corresponds to the relationship between the vector of nodal forces and the vector of nodal displacements, such as:

$$
\begin{pmatrix}
-N_1(0) \\
-N_2(0) \\
N_1(\Delta) \\
N_2(\Delta) \\
-V_1(0) \\
-V_2(0) \\
V_1(\Delta) \\
V_2(\Delta) \\
-M_1(0) \\
-M_2(0) \\
M_1(\Delta) \\
M_2(\Delta)
\end{pmatrix}
= K_{BBe}
\begin{pmatrix}
u_1(0) \\
u_2(0) \\
u_1(\Delta) \\
u_2(\Delta) \\
v_1(0) \\
v_2(0) \\
v_1(\Delta) \\
v_2(\Delta) \\
\theta_1(0) \\
\theta_2(0) \\
\theta_1(\Delta) \\
\theta_2(\Delta)
\end{pmatrix}
\tag{58}
$$

The fundamental matrix of A, termed Φ_A, is computed at $X=0$ and $X=\Delta$; using the MATLAB software, the associated command is "expm":

$$
\begin{cases}
\Phi_A(X = 0) = expm(A.0) \\
\Phi_A(X = \Delta) = expm(A.\Delta)
\end{cases}
\tag{59}
$$

From these two 12*12 matrices, two matrices M' and N' are extracted. M' (N') is composed of the lines related to the nodal displacements (forces). For each, a first block of six lines and twelve rows comes from $\Phi_A(X=0)$ and the second block of six lines and twelve rows comes from $\Phi_A(X=\Delta)$, such that:

$$
\begin{cases}
M' = \Phi_U(0,\Delta) = \begin{pmatrix} [\Phi_A(X=0)]_{i=1,2,3,4,5,6\ ;j=1:12} \\ [\Phi_A(X=\Delta)]_{i=1,2,3,4,5,6\ ;j=1:12} \end{pmatrix} \\
N' = \Phi_F(0,\Delta) = \begin{pmatrix} [\Phi_A(X=0)]_{i=7,8,9,10,11,12\ ;j=1:12} \\ [\Phi_A(X=\Delta)]_{i=7,8,9,10,11,12\ ;j=1:12} \end{pmatrix}
\end{cases}
\tag{60}
$$

where i (j) indicates the line (row) number. As K_{BBe} is defined according to ($[u_1(0)\ u_2(0)\ u_1(\Delta)$ $u_2(\Delta)\ v_1(0)\ v_2(0)\ v_1(\Delta)\ v_2(\Delta)\ \theta_1(0)\ \theta_2(0)\ \theta_1(\Delta)\ \theta_2(\Delta)]$), a simple rearrangement of the order of

lines of *M'* is performed to produce the matrix *M*. Similarly, the matrix *N'* is subjected to the same operation. In a similar way, the terms related to nodal forces at *X=0* are multiplied by -1 to follow the arrangement (*[-N₁(0) -N₂(0) N₁(Δ) N₂(Δ) -V₁(0) -V₂(0) V₁(Δ) V₂(Δ) -M₁(0) -M₂(0) M₁(Δ) M₂(Δ)]*). It leads to the definition of the matrix *N*. The elementary stiffness matrix K_{BBe} is equal to the product of *N* and the inverse of *M*: $K_{BBe}=N.M^{-1}$. The stiffness matrix of the beam element under a local equilibrium coupling the in-plane and out-of-plane load is described in Appendix C. As for the 1D-bar analysis, the minimization of the potential energy leads to a linear system the size of which is *(6n_ME+12)²*.

Even if it is not the topic of this paper, it is obvious that this previous approach can be easily used to develop ME including different number of layers of adhesives and adherends (e.g. double lap joint configuration), various beam models (e.g. Timoshenko beam model, see Appendix D) or taking into account for a linear variation of shear stress in the adherend thickness following [28] (see Appendix D).

3. Comparative study

3.1. Overview

A comparative study of the ISLM by Stein et al. [22], the present 1D-bar TEPS, 1D-bar ME and 1D-beam ME analysis is presented in this section, starting with a convergence study. This study is performed against three test cases (TCs):

(i)   TC#1: a balanced joint configuration under a pure mechanical load;

(ii)   TC#2: an unbalanced joint configuration under a pure thermal load;

(iii)   TC#3: an unbalanced joint configuration under combined mechanical and thermal loads.

The joint configurations are almost inspired from to those found in [19,22]. The mechanical load is *F=5 kN* while the thermal load is *Δ_T=+50°K*. The balanced joint configuration is made

of two steel adherends. The unbalanced joint configuration has the same geometry as the balanced one, but the lower adherend is made in aluminum instead of steel. The geometrical and mechanical parameters are given in Table 1 and Table 2 respectively in accordance to Figure 2 and Figure 6. A parabolic graduation of adhesive properties is assumed such as:

$$E_a(x) = E_{a,max}(x) - \left(E_{a,max}(x) - E_{a,min}(x)\right)\left(\frac{x}{c}\right)^2 \tag{61}$$

$$G_a(x) = G_{a,max}(x) - \left(G_{a,max}(x) - G_{a,min}(x)\right)\left(\frac{x}{c}\right)^2 \tag{62}$$

where $E_{a,max}$ ($E_{a,min}$) is the maximal (minimal) adhesive peel modulus in the graduation and $G_{a,max}$ ($G_{a,min}$) is the maximal (minimal) adhesive shear modulus in the graduation. In this work, the ratio between the maximal (minimal) adhesive peel modulus and the maximal (minimal) adhesive shear modulus through is constant and equal to $2(1+ v_a)$, where v_a is the adhesive Poisson's ratio. In this work, the adhesive peel modulus is then represented by the adhesive Young's modulus. The adhesive properties are then summarized in Table 3.

Table 1. Geometrical parameters of joint configurations

b (mm)	e_a (mm)	$e_1=e_2$ (mm)	L (mm)	$l_1=l_2$ (mm)
25	0.2	2	25	75

Table 2. Material parameters of adherends.

	Coefficient of thermal expansion (K^{-1})	Young's modulus (GPa)
steel	12E-6	210
aluminum	24E-6	70

Table 3. Adhesive material properties.

$E_{a,max}$ (MPa)	$E_{a,min}$ (MPa)	v_a

24

6500	2500	0.36

3.2.   Convergence study

The convergence study is performed on the TC#1 and the TC#2 (FGA balanced joint under pure mechanical load and pure thermal load). The resolution scheme based on TEPS needs to truncation order (*n_max*) while the one based on the ME technique needs a mesh with *n_ME* BBa or BBe. A convergence study is then performed by recording the maximal adhesive stresses as a function *n_max* and *n_ME*.

The maximal adhesive shear stress (T_{max}) is provided in Figure 8 as function of the order of series truncation (*n_max*) for both TC#1 and TC#2 as predicted by the ISLM and the TEPS analysis. It is shown that T_{max} tends to a finite value (12.56 MPa for TC#1 and 11.11 MPa for TC#2) for an order of series truncations lower than *n_max=20*. For the case of *n_max=100* with the TEPS analysis, the ratio between each series term U_n with the sum of series terms – which is equal to *Δu(x=c)* – is provided in Figure 9 for both TC#1 and TC#2, illustrating the fast convergence of series. Moreover, the TEPS analysis provides a maximal adhesive shear stress relatively different of 1.68E-4 % from the one provided by the ISLM (for TC#1).
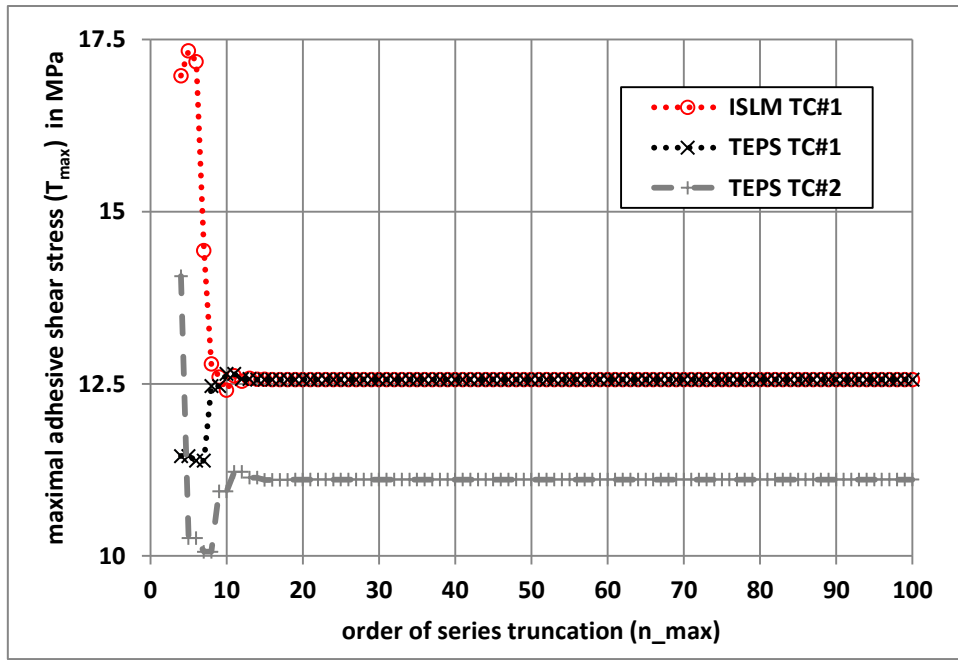
Figure 8. Maximal adhesive shear stress as function the order of series truncation for the ISLM by Stein et al. [22] and the 1D-bar TEPS analysis for both TC#1 and TC#2.
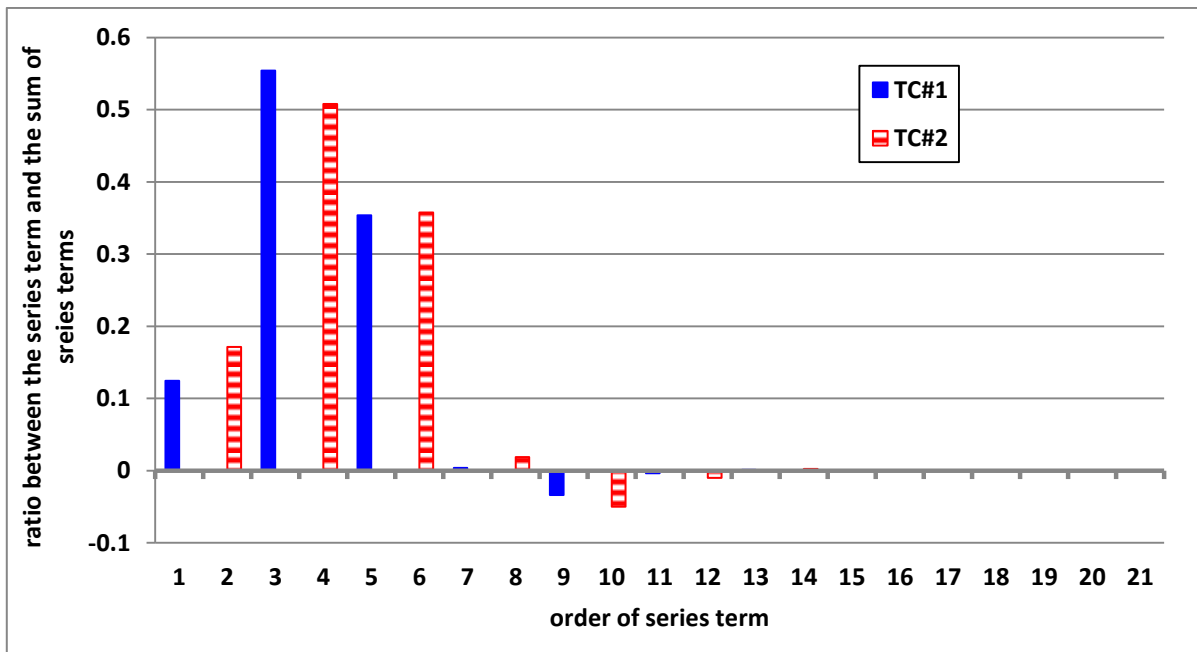
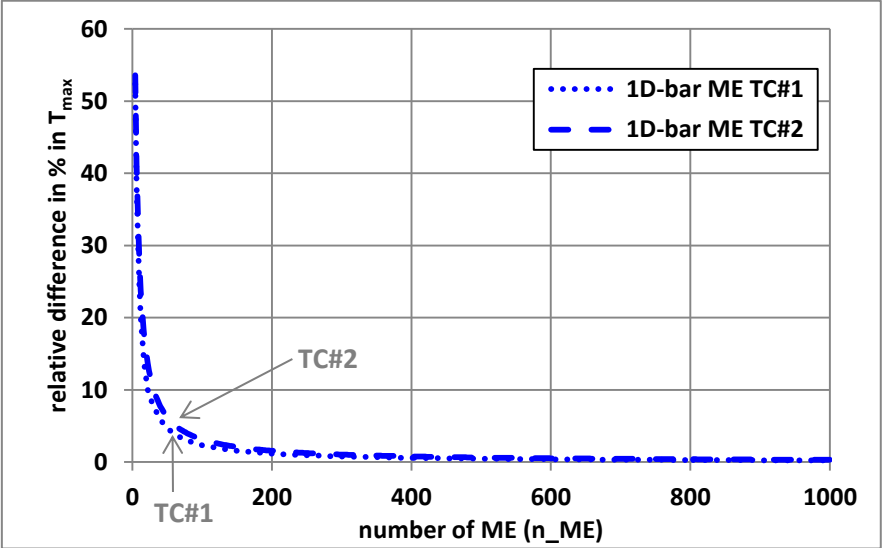Figure 9. Ratio between each series term and the sum of series terms for both TC#1 and TC#2.

The relative difference in the maximal adhesive provided the 1D-bar ME analysis from the one by 1D-bar TEPS analysis as function of the number of MEs for both TC#1 and TC#2 is provided in Figure 10. It is shown that T_{max} provided by the 1D-bar ME analysis tends to the one provided by the TEPS analysis when the number of MEs is increased. For $n\_ME=1000$, the relative difference is 0.16% (0.22%) for TC#1 (TC#2). As a result, the TEPS resolution scheme is less costly in terms of CPU time than the ME one, since convergence is obtained at a lower size of the linear system to be inverted. This behavior is related to the meshing strategy associated with the graduation of adhesive properties. It is thought that the number of MEs could be reduced by adapting the length of each ME according to the current gradient of adhesive properties for example. However, the mesh optimization is not the topic of this paper. In Figure 11, the maximal adhesive shear stress provided by the 1D-bar and 1D-beam analysis as function the order of the number of MEs for both TC#1 and TC#2 is provided. As expected from Figure 10, it is shown that T_{max} tends to a finite value.

Figure 10. Relative difference in % in the maximal adhesive provided the 1D-bar ME analysis from the one by 1D-bar TEPS analysis as function of the number of MEs for both TC#1 and TC#2.
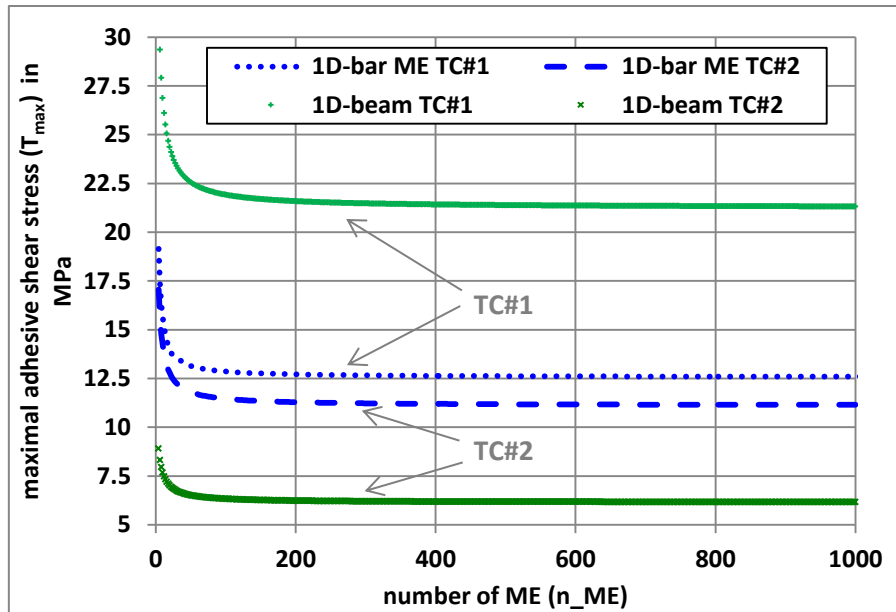
Figure 11. Maximal adhesive shear stress provided by the 1D-bar and 1D-beam analysis as function the order of the number of MEs for both TC#1 and TC#2.

3.3. Elements of validation

The ME technique is a particular resolution scheme allowing for the system of ODEs coming from simplifying hypotheses on which various models – such as Volkersen, Goland and Reissner, Hart-Smith, Luo and Tong – are based. It was shown in that, for bonded joints with constant adhesive properties under mechanical or thermal loads, the predictions from the models using the ME resolution scheme provide the same results as those provided by the related reference models [36-40]. In other words, the same hypotheses lead to the same results. Moreover, it was shown that the predictions from the ME analysis are in close agreements with those from FE models built on bar or beam element linked by peel and/or shear springs, under mechanical and/or thermal loads, involving the update of adhesive properties for each ME to take into account for nonlinear adhesive material behaviors [39-40]. These FE models were developed to be the most representative for the ME analysis in order to validate the codes. As a result, the ME resolution scheme provide validated predictions relevant to the simplifying hypotheses. Similarly, the TEPS resolution scheme allows for the

resolution of differential equations related to the simplifying equations. It was validated and assessed in the case of FGA single-lap joints under mechanical load by Stein et al. [22].

In addition, the stress distributions at constant maximal and minimal adhesive properties are then provided from the use of ME models in the following sections. An order of truncation equal to 100 and a number of MEs equal to 500 is chosen in the following sections.

Considering the balanced joint configuration in the frame of the 1D-bar analysis, the adhesive shear stress distributions along the overlap are provided in Figure 12. The predictions considering homogeneous shear modulus $G_{a,min}$ and $G_{a,max}$, as well as those from ISLM by Stein et al. [22], the present 1D-bar TEPS and ME analyses are included. It appears that the predictions from the ISLM, the TEPS analysis and 1D-bar ME analysis provide the same predictions.
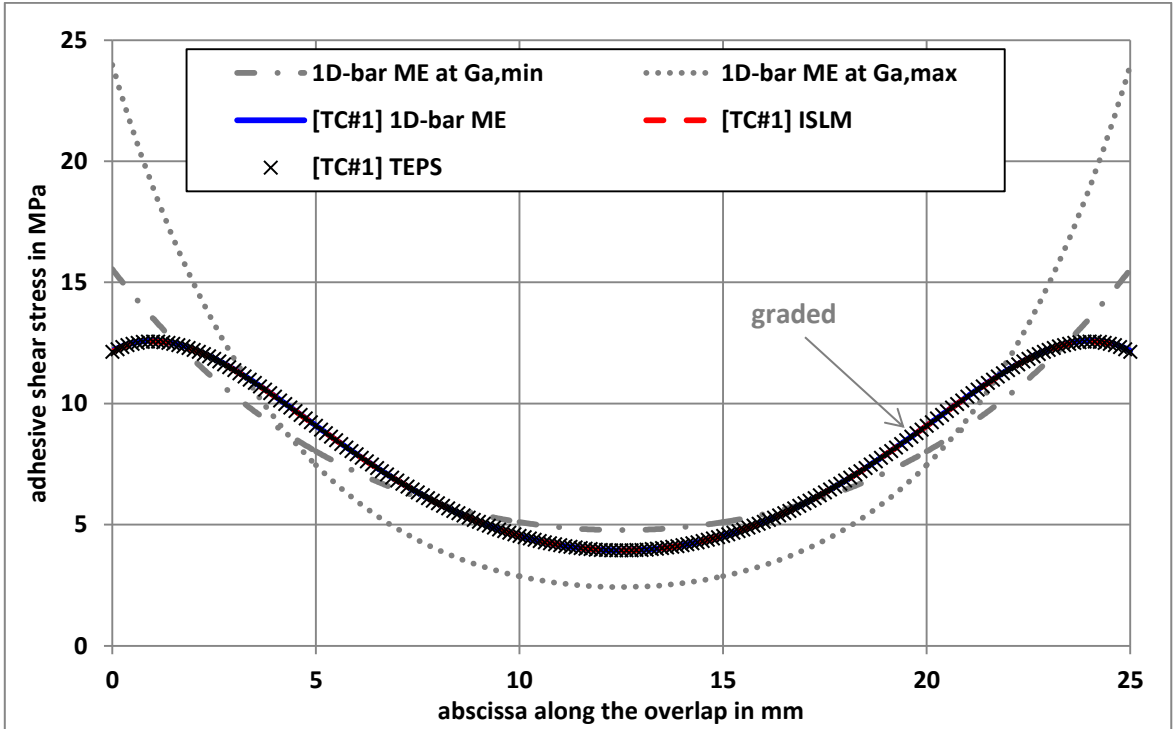
Figure 12. Adhesive shear stress distribution along the overlap associated with TC#1 for the

1D-bar analyses.

Considering the balanced joint configuration in the frame of the 1D-beam analysis, the adhesive shear and peel stress distributions along the overlap are provided in Figure 13 and

Figure 14, respectively. The predictions considering homogeneous shear and peel modulus $(G_{a,min}\,; E_{a,min}\,)$ and $(G_{a,max}\,; E_{a,max}\,)$, as well as those from GM by Stein et al. [22], the present 1D-beam ME analyses are included. As the simplifying hypotheses of the GM differ from those used in the present 1D-beam analysis solved with the ME technique, the predictions from the GM and 1D-beam ME analysis are not superimposed. Nevertheless, it appears that the predictions are close each other and qualitatively similar. As expected, the predictions in terms of adhesive shear stress by the 1D-bar analysis differ from those by the 1D-beam analysis.
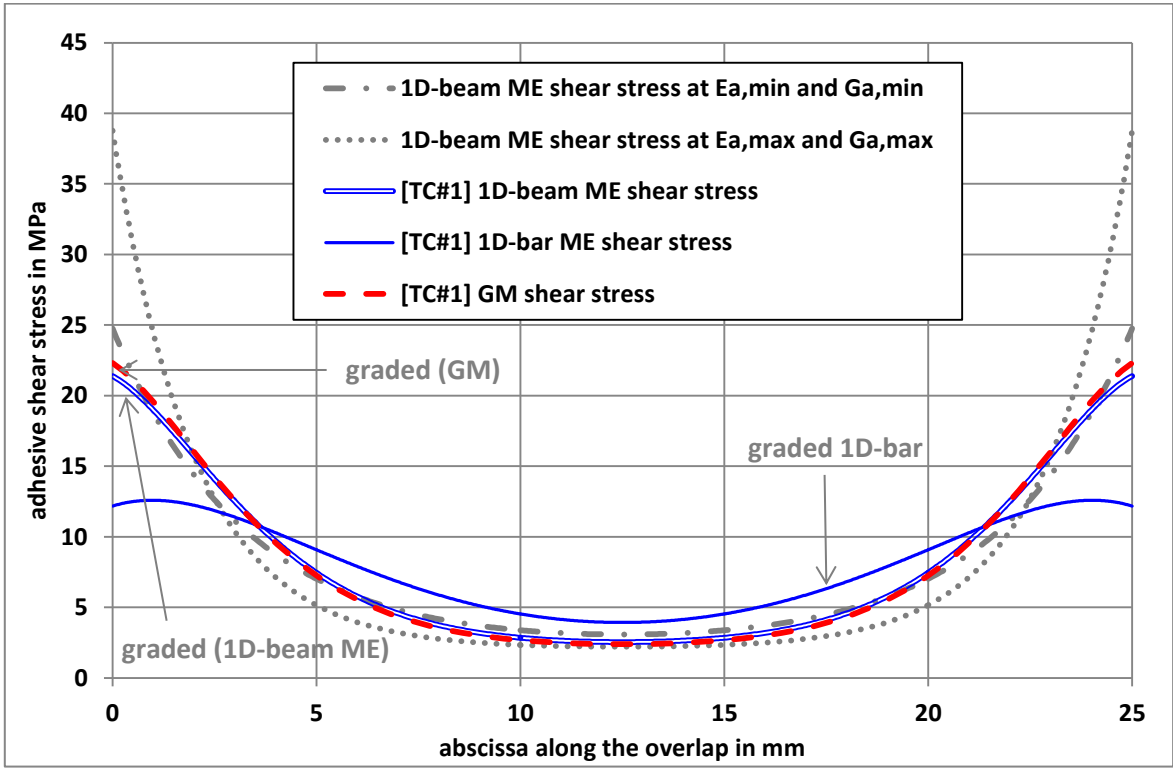
Figure 13. Adhesive shear stress distribution along the overlap associated with TC#1 for the 1D-beam analyses.
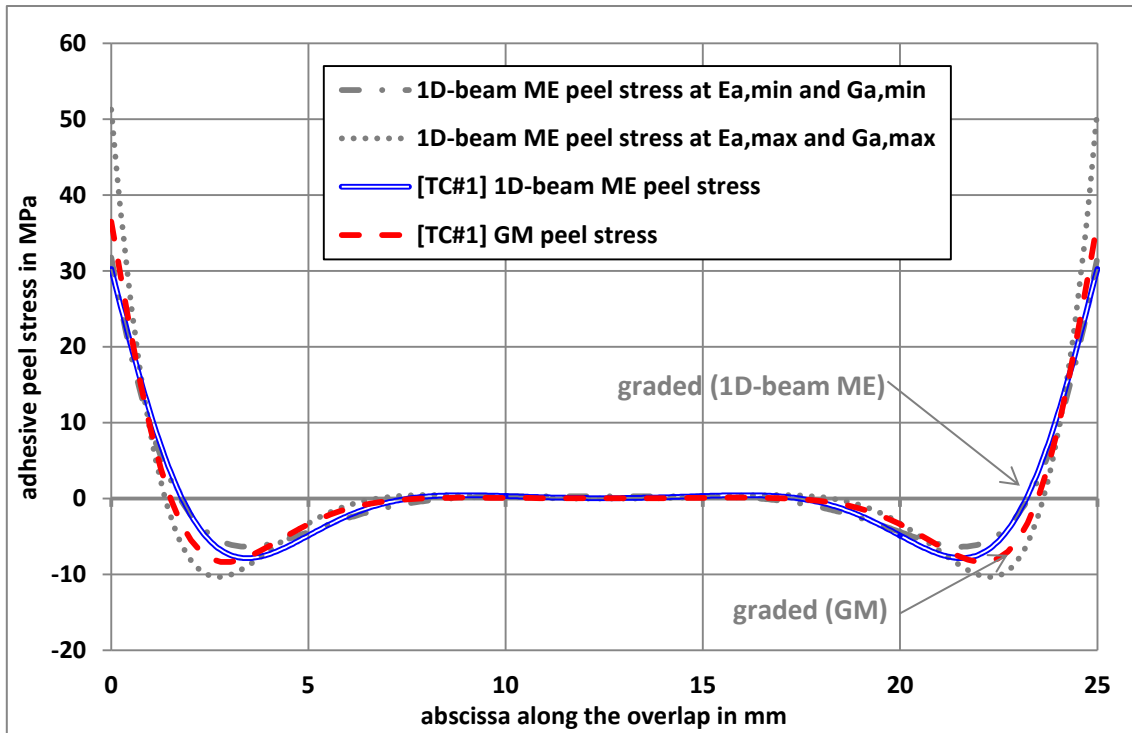
Figure 14. Adhesive peel stress distribution along the overlap associated with T C#1 for the 1D-beam analyses.

3.4. Test cases

3.4.1 1D-bar analyses

The adhesive shear stress distributions along the overlap are provided in Figure 15 and Figure 16 for the 1D-bar analyses for TC#2 and TC#3 (unbalanced joint configuration under combined mechanical and thermal loads), respectively. The ISLM cannot then be applied. It is shown that the predictions by the 1D-bar TEPS and ME analyses are superimposed. For each case, the graduation of adhesive properties allows to reduce the peak stresses below those obtained from the case at constant minimal shear modulus. However, the reduction is less pronounced for the unbalanced cases (TC#2 and TC#3). For the TC#1, the reduction in adhesive shear peak stress at $x=c$ of the FGA joint is -21.7% from the bonded joints with a constant shear modulus $G_{a,min}$, while it is -14.5% (-15.3%) for TC#2 (TC#3).
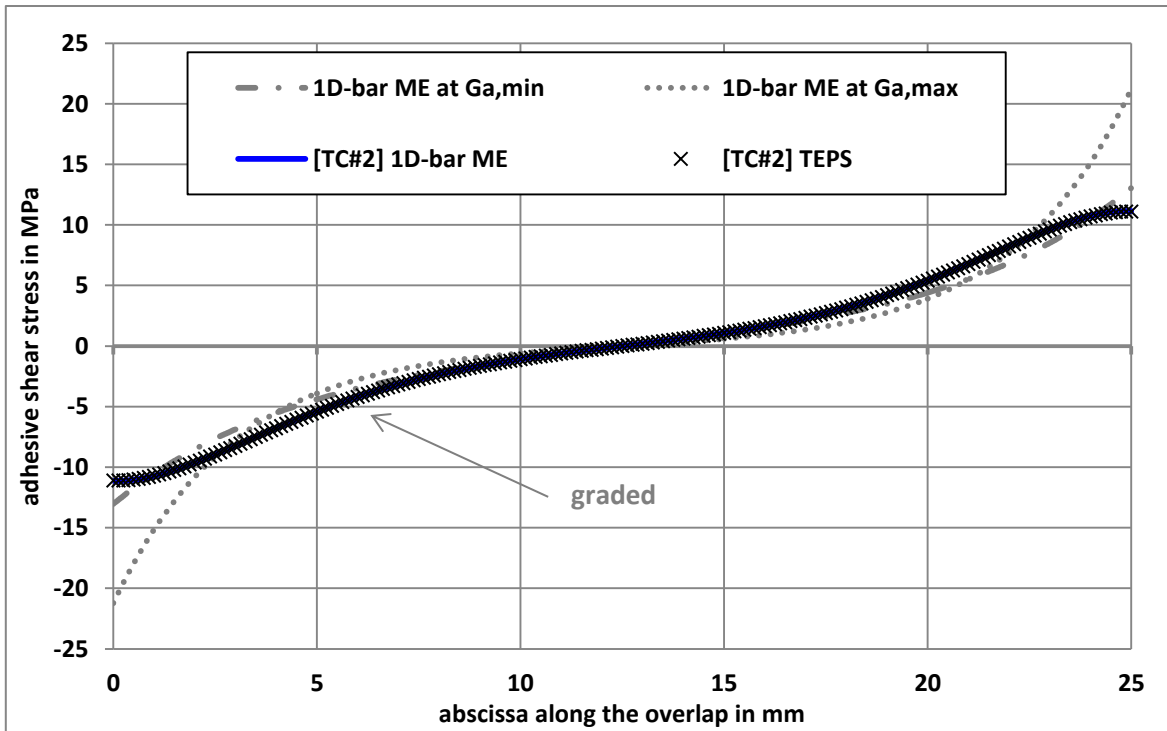
Figure 15. Adhesive shear stress distribution along the overlap associated with TC#2 for the
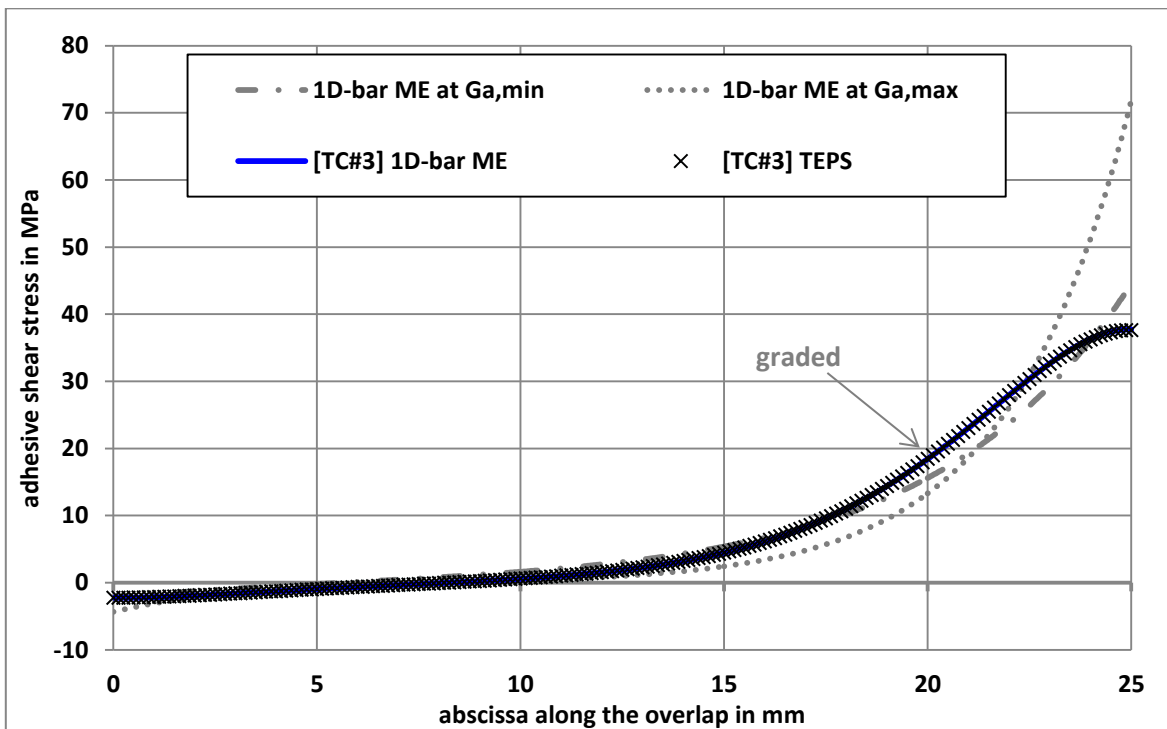
1D-bar analyses.

Figure 16. Adhesive shear stress distribution along the overlap associated with TC#3 for the

1D-bar analyses.

3.4.2 1D-beam analyses

In the frame of 1D-beam analysis, the adhesive shear and peel stress distributions along the overlap are provided in Figure 17 to Figure 18, and in Figure 19 to Figure 20, for TC#2 and TC#3 respectively. The predictions come from the 1D-beam ME analysis only since the GM cannot be applied for these TCs. The adhesive shear stress distribution along the overlap of FGA joints from the 1D-bar analysis differs significantly from the one from 1D-beam analysis. As for the 1D-bar analysis, the reduction of adhesive peak stresses is shown while the stress distribution of FGA joints appears close to the one of the bonded joints with minimal and constant adhesive modulus. For TC#1, the reduction in adhesive shear stress at $x=c$ for the FGA joint is -13.6% from the bonded joints with a constant minimal Young and shear modulus, while it is -10.0% (-9.61%) for TC#2 (TC#3). Similarly, in terms of peel stress at $x=c$, the reduction is -4.85% (-2.59%) for TC#1 (TC#3).
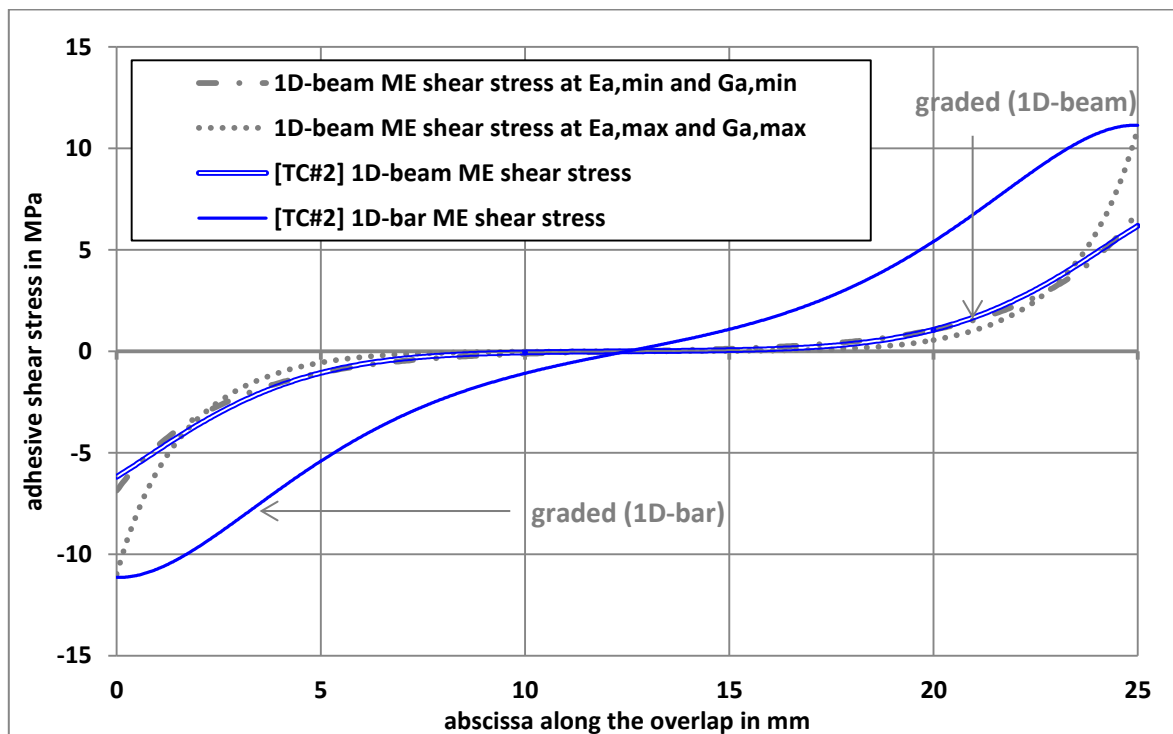

Figure 17. Adhesive shear stress distribution along the overlap associated with TC#2 for the 1D-beam analyses.
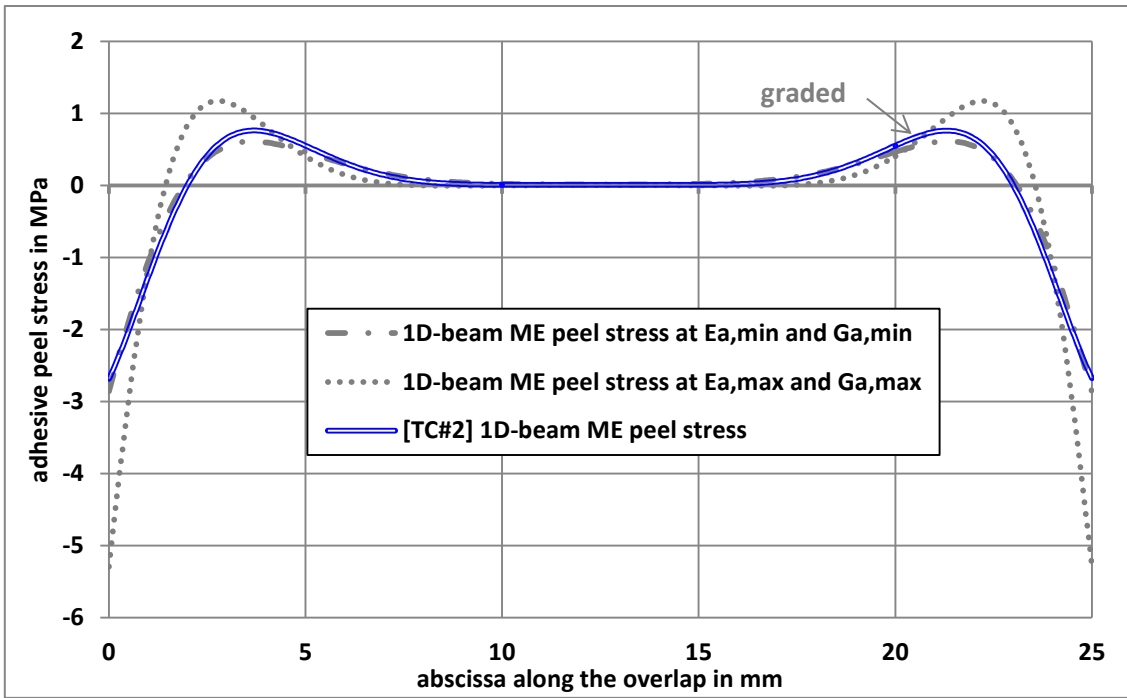
Figure 18. Adhesive shear stress distribution along the overlap associated with TC#2 for the
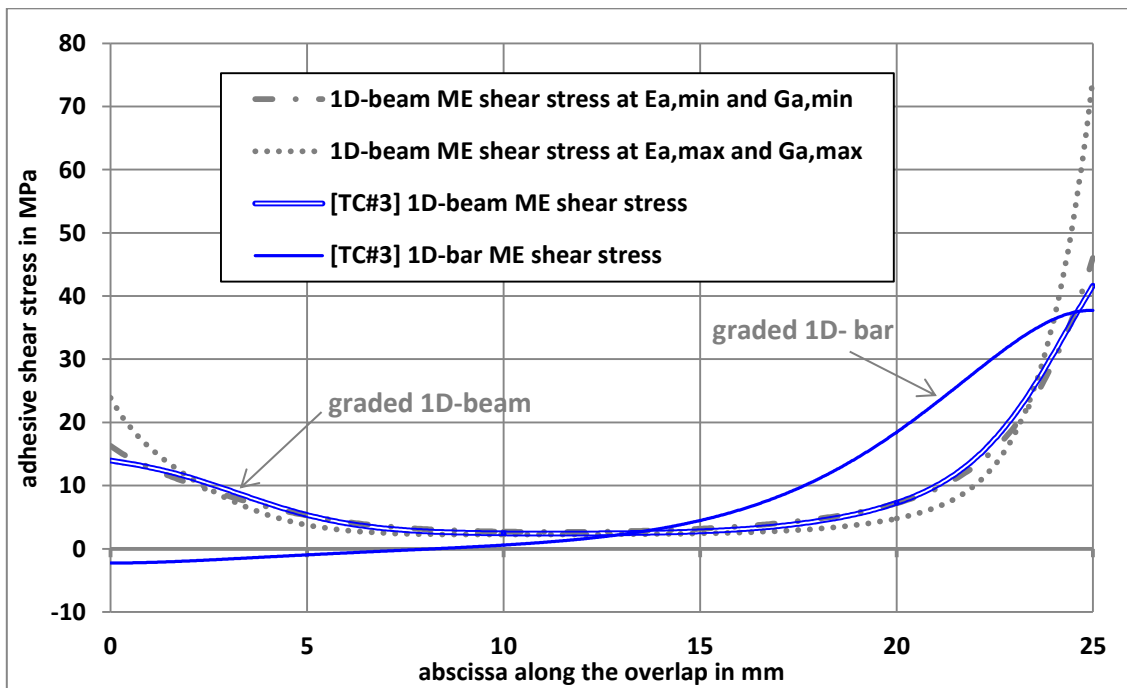
1D-beam analyses.

Figure 19. Adhesive peel stress distribution along the overlap associated with TC#3 for the
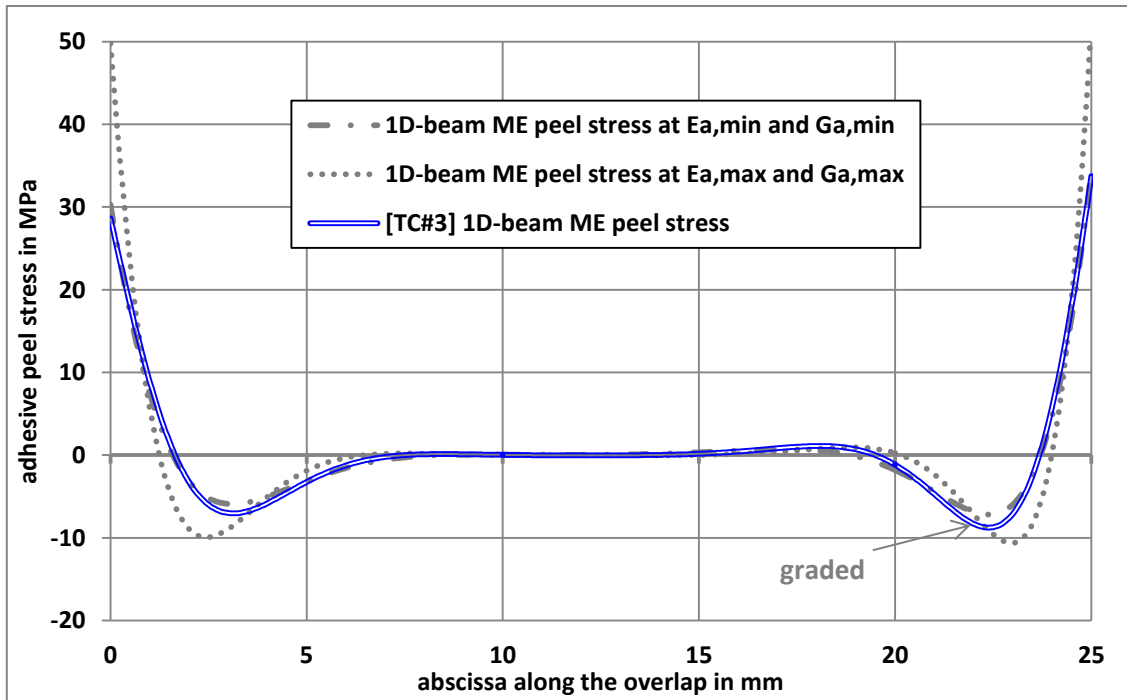
1D-beam analyses.

Figure 20. Adhesive peel stress distribution along the overlap associated with TC#3 for the

1D-beam analyses.

3.5.   Reduction of adhesive peak stresses

This section aims at illustrating how the use of the 1D-beam ME analyses could help in the

design of adhesive graduation to reduce the adhesive peak stresses, for the unbalanced joint

configuration subjected to pure thermal load and combined mechanical and thermal loads in

particular. According to Hart-Smith [1,24], the adhesive peel stress could lead to an

anticipated failure of single-lap bonded joint, whereas the potential of shear deformation is

not reached. For the unbalanced joint configuration, under a pure thermal load, it is shown

that the level of adhesive peel stresses remain very low (see Figure 18), while the adhesive

shear stress are symmetrical in absolute value (see Figure 17). Under combined mechanical

and thermal loads, the level of adhesive peel stress is significantly higher due to the

introduction of the mechanical load inducing a bending moment at both overlap ends (see

Figure 20). Moreover, even if the adhesive peel stress distribution is asymmetrical due to the

unbalance of the joint, the adhesive peel peaks stresses located at both overlap ends are significant. As a result, for both previous load cases, a symmetrical adhesive graduation is kept in order to try to reduce the adhesive peak stresses. It is assumed to follow a symmetrical power law parametrized by p, with $p=1,2,3,4$, such as:

$$E_a(x) = E_{a,max}(x) - \left(E_{a,max}(x) - E_{a,min}(x)\right)\left(\frac{x}{c}\right)^{2p} \tag{63}$$

$$G_a(x) = G_{a,max}(x) - \left(G_{a,max}(x) - G_{a,min}(x)\right)\left(\frac{x}{c}\right)^{2p} \tag{64}$$

The increase of the parameter p allow for the enlargement of the overlap length at higher modulus, while increasing the graduation slope at both overlap ends where the adhesive stress gradients are higher. The shape of various graduations is illustrated in Figure 21.
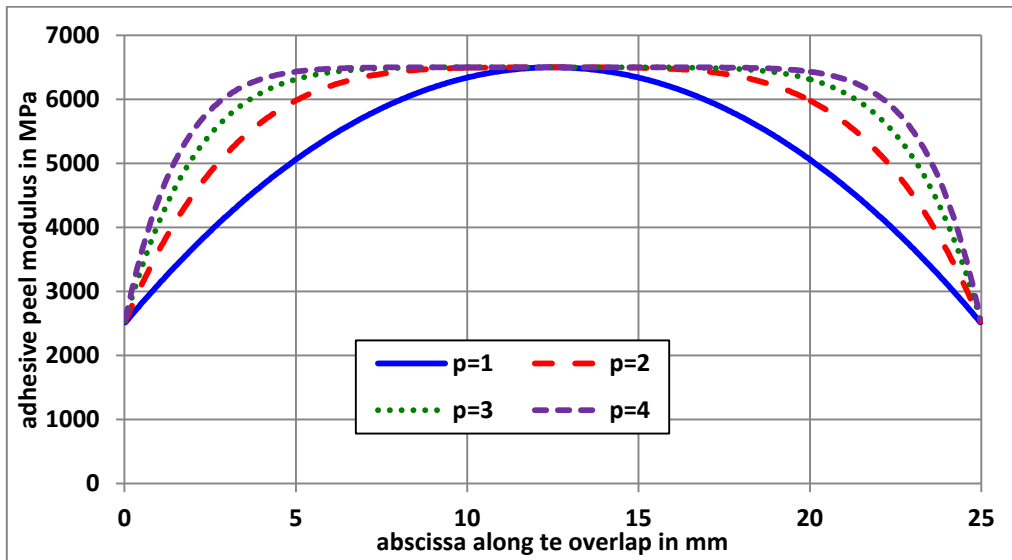
Figure 21. Adhesive peel modulus along the overlap as a function of *p*.

Under a pure thermal load, the adhesive shear and peel stress distributions along the overlap are provided in Figure 22 to Figure 23, respectively. It is shown that the level of adhesive peel stresses remain low along the overlap. Relatively to the adhesive shear peak stresses with *p=1*, a reduction of -5.13%, -4.56% and -1.78% is obtained with *p=2*, *p=3* and *p=4* respectively. Relatively to the adhesive stress at overlap end, where the level of adhesive peel

stress is the highest, the reductions obtained become -5.22%, -8.42% and -10.6% with *p=2*, *p=3* and *p=4* respectively. The choice of adhesive graduation law associated higher power order allows then for a lag of the adhesive shear peak stress in direction of the center of the overlap.
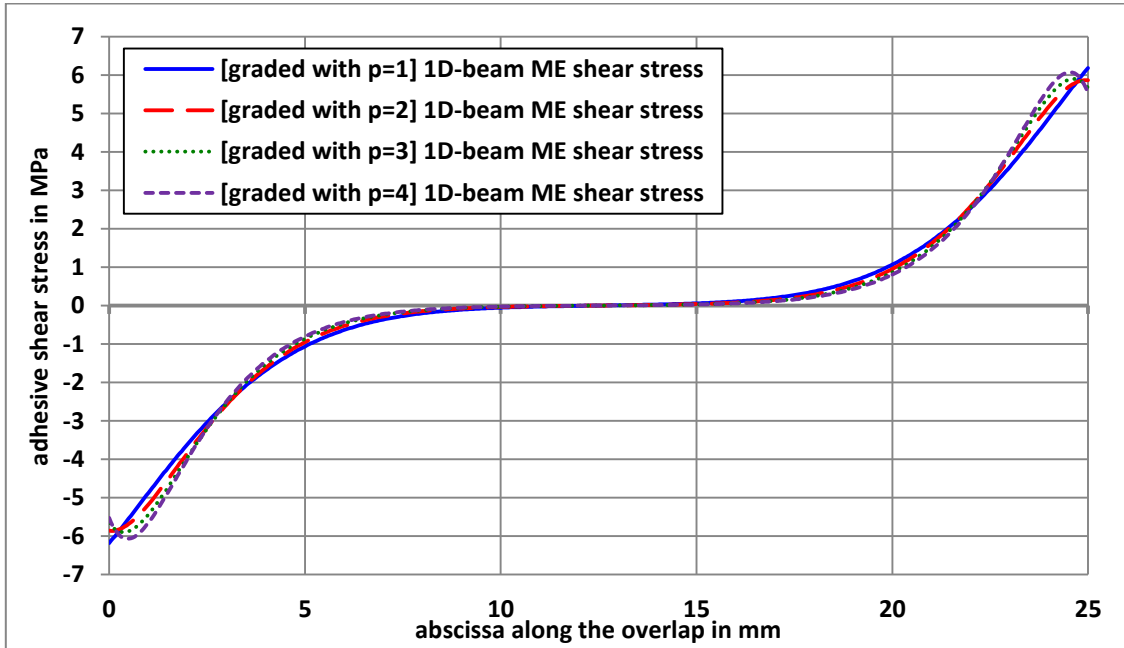

Figure 22. Adhesive shear stress distribution along the overlap for the unbalanced joint configuration under a pure thermal load, for various adhesive graduations.
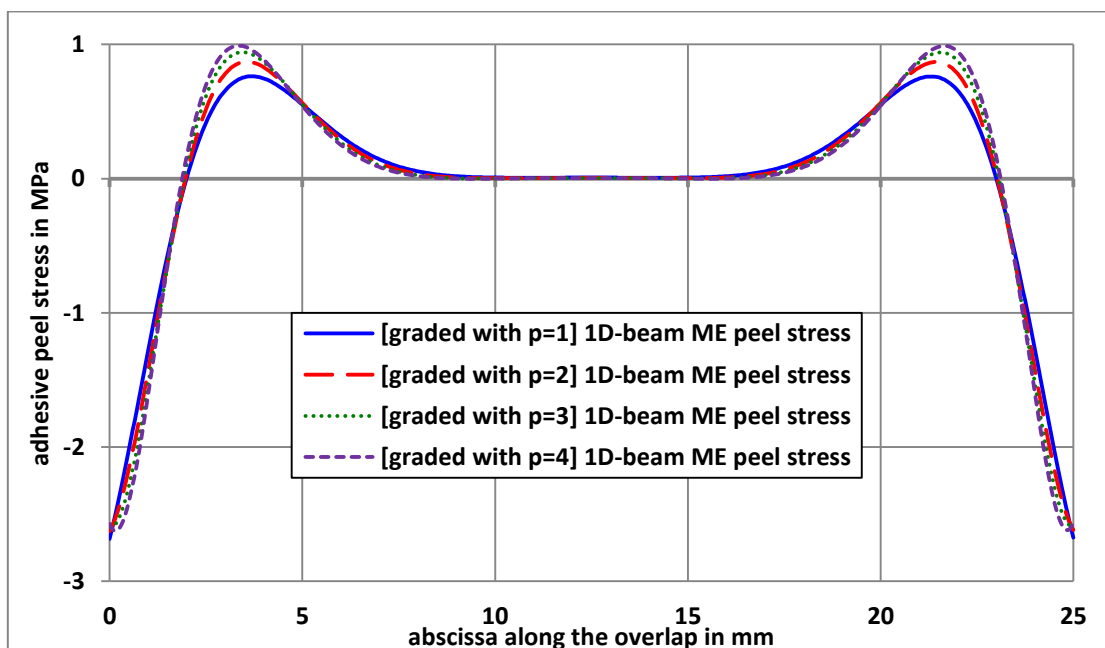
. Adhesive peel stress distribution along the overlap for the unbalanced joint configuration under a pure thermal load, for various adhesive graduations.

Under a combined mechanical and thermal load, the adhesive shear and peel stress distributions along the overlap are provided in Figure 24 to Figure 25, respectively. As for the pure thermal load case, the adhesive peak shear stresses are not located at both overlap ends for $p=2$, $p=3$ and $p=4$. Relatively to the adhesive shear peak stresses with $p=1$ a reduction of -4.80%, -5.39% and -3.18% is obtained with $p=2$, $p=3$ and $p=4$ respectively. Relatively to the adhesive stress at overlap end, where the level of adhesive peel stress is the highest, the reductions obtained become -4.80%, -7.76% and -9.77% with $p=2$, $p=3$ and $p=4$ respectively. The adhesive peak peel stresses are located at both overlap ends; the maximal peak is located at $x=c$. It is shown that with $p=2$, $p=3$ and $p=4$ respectively, both peaks at overlap ends are reduced. Relatively to the adhesive peel peak stresses at $x=c$ with $p=1$, a reduction of -2.87%, -4.91% and -6.45% is obtained with $p=2$, $p=3$ and $p=4$ respectively
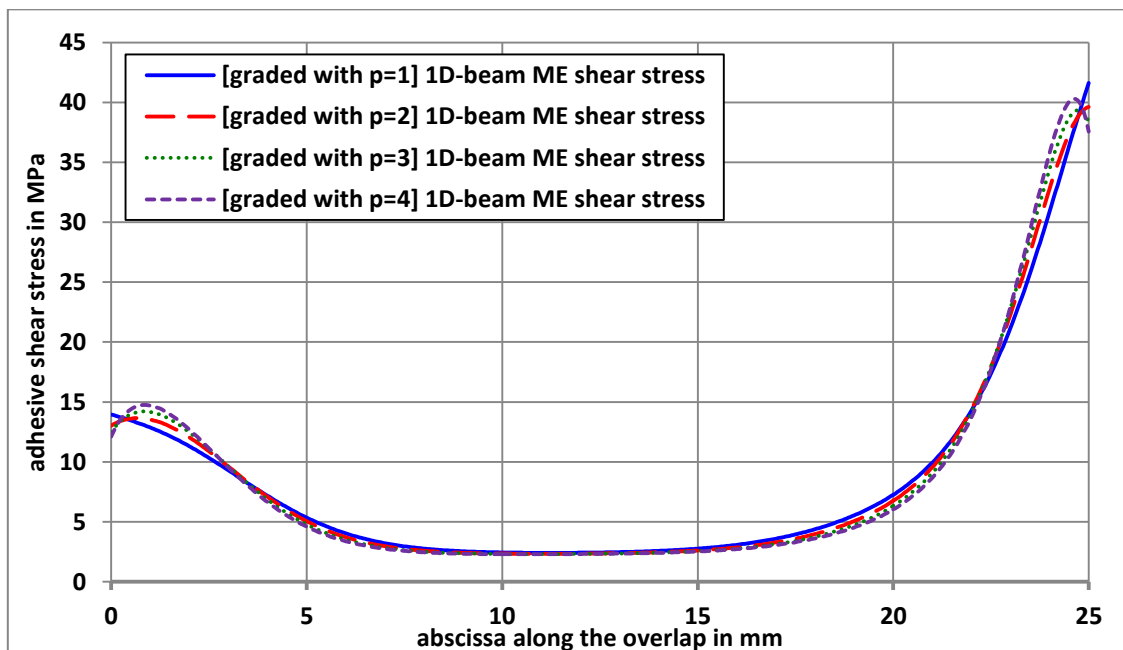
Figure 24. Adhesive shear stress distribution along the overlap for the unbalanced joint configuration under combined mechanical and thermal loads, for various adhesive graduations.
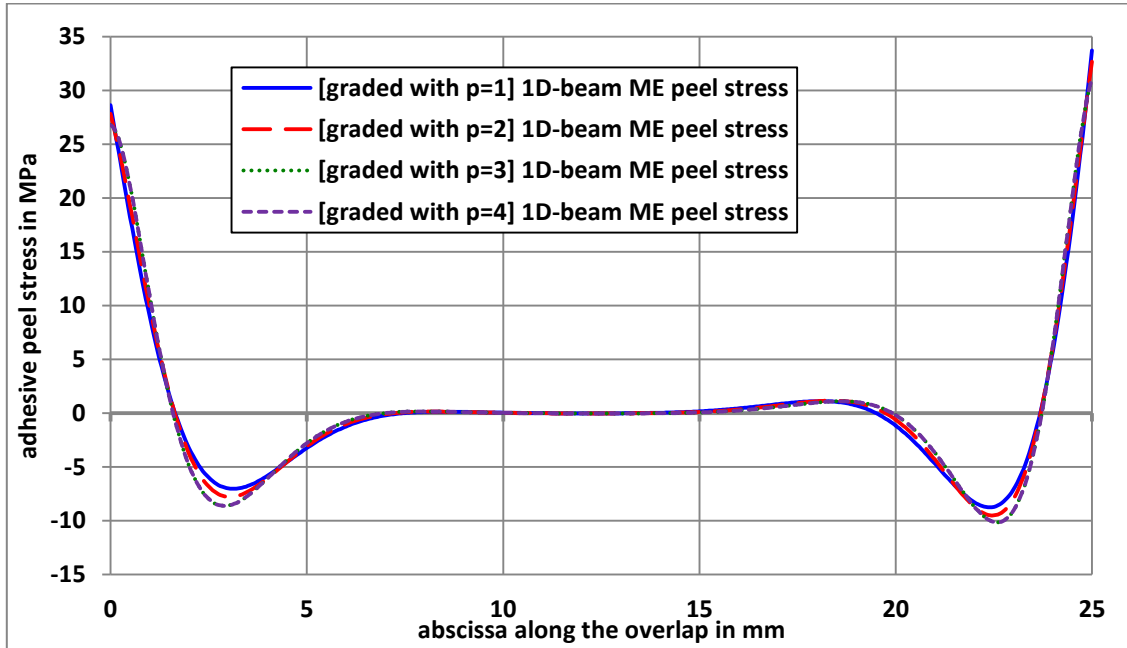

Figure 25. Adhesive peel stress distribution along the overlap for the unbalanced joint configuration under combined mechanical and thermal loads, for various adhesive graduations.

4.   Conclusions

In this paper, simplified stress analyses for FGA (functionally graded adhesive) joints under combined mechanical and thermal loads are presented in order to predict the adhesive stress distribution along the overlap as a function of the adhesive graduation. The graduation of the adhesive properties leads to differential equations which coefficients can vary the overlap. For the 1D-bar analyses, two different resolution schemes are employed. The first one makes use of Taylor expansion power series (TEPS) as already published under pure mechanical load. The second one is based on the macro-element (ME) technique. For the 1D-beam analysis, the resolution is only based on the ME technique. A comparative study, including a convergence

study, is presented on balanced and unbalanced joint configuration under pure mechanical, pure thermal and combined mechanical and thermal loads. The following conclusions could then be made:

- the present 1D-bar TEPS analysis restricted to a pure mechanical load provide the same results as the ISLM by Stein et al [22];

- the present 1D-bar TEPS and the 1D-bar ME analysis provide the same results;

- the use of TEPS resolution scheme provides converged results at lower CPU cost than the ME resolution scheme;

- the graduation of the adhesive properties allows for the reduction of adhesive peak stresses;

- the present 1D-beam ME analysis restricted to a pure mechanical load provide similar results as the GM by Stein et al [22];

- the reduction of the adhesive shear peak stresses is found less pronounced when the 1D-beam analysis is used instead of the 1D-bar analysis;

- the reduction of the adhesive peak stresses in less pronounced for an unbalanced joint than for a balance joint.

- higher level of reduction can be obtained by modifying the graduation law.

A dedicated validation campaign based on FE modelling should be undertaken in order to assess the relevance of the simplifying hypotheses and the performance of the resolution scheme for the stress analysis of FGA joints. In particular, the free stress state at both overlap ends cannot be captured with the simplifying hypotheses used. Besides, optimization processes could be used to optimize the graduation of adhesive properties as function of the adhesive stress distribution to minimize the adhesive peak stresses. Finally, in order to increase the strength of FGA single-lap joints, an idea could be to graduate the properties of both the adhesive and adherends. For example, the reduction of adhesive peel stresses at both

40

overlap ends could be obtain by tapering the adherend edge, while increasing the ratio between the overlap length and the adherend thickness [1].

Acknowledgement

Appendix A

This appendix presents the mathematical description of the elementary stiffness matrix of the BBa element. Equation Eq. (7) can be explicitly written such as a system of a coupled second order ODE at constant coefficients:

$$\begin{cases} \frac{d^2 u_1}{dX^2} + k_{II} \frac{1}{e_1 E_1}(u_2 - u_1) = 0 \\ \frac{d^2 u_2}{dX^2} + k_{II} \frac{1}{e_2 E_2}(u_2 - u_1) = 0 \end{cases} \tag{A-1}$$

This system is solved such as:

$$u_1(X) = \frac{1}{2}(c_1 + c_2 X - c_3(1+\chi)e^{-\eta X} - c_4(1+\chi)e^{\eta X}) \tag{A-2}$$

$$u_2(X) = \frac{1}{2}(c_1 + c_2 X + c_3(1-\chi)e^{-\eta X} + c_4(1-\chi)e^{\eta X}) \tag{A-3}$$

with:

$$\chi = \frac{\psi^2}{\eta^2} \tag{A-4}$$

$$\psi^2 = \frac{G}{e}\left(\frac{1}{e_1 E_1} - \frac{1}{e_2 E_2}\right) \tag{A-5}$$

$$\eta^2 = \frac{G}{e}\left(\frac{1}{e_1 E_1} + \frac{1}{e_2 E_2}\right) \tag{A-6}$$

where c_1, c_2, c_3 and c_4 are integration constants. The boundary conditions at both extremities of the BBa element, in terms of displacements, lead to the expressions for the integration constants as functions of nodal displacements u_i, u_j, u_k and u_l (see Figure 4):

$$c_1 = (1-\chi)u_i + (1+\chi)u_j \tag{A-7}$$

$$c_2 = -\frac{(1-\chi)}{\Delta}u_i - \frac{(1+\chi)}{\Delta}u_j + \frac{(1-\chi)}{\Delta}u_k + \frac{(1+\chi)}{\Delta}u_l \tag{A-8}$$

$$c_3 = -\frac{e^{\eta\Delta}}{2\sinh\eta\Delta}u_i + \frac{e^{\eta\Delta}}{2\sinh\eta\Delta}u_j + \frac{1}{2\sinh\eta\Delta}u_k - \frac{1}{2\sinh\eta\Delta}u_l \tag{A-9}$$

$$c_4 = \frac{e^{-\eta\Delta}}{2\sinh\eta\Delta}u_i - \frac{e^{\eta-\Delta}}{2\sinh\eta\Delta}u_j - \frac{1}{2\sinh\eta\Delta}u_k + \frac{1}{2\sinh\eta\Delta}u_l \tag{A-10}$$

It can then be written under this shape:

$$C = \begin{pmatrix} c_1 \\ c_2 \\ c_3 \\ c_4 \end{pmatrix} = M_e^{-1} U_e \tag{A-11}$$

With:

$$M_e^{-1} = \begin{pmatrix} (1-\chi) & (1+\chi) & 0 & 0 \\ -\frac{(1-\chi)}{\Delta} & -\frac{(1+\chi)}{\Delta} & \frac{(1-\chi)}{\Delta} & \frac{(1+\chi)}{\Delta} \\ -\frac{e^{\eta\Delta}}{2\sinh\eta\Delta} & \frac{e^{\eta\Delta}}{2\sinh\eta\Delta} & \frac{1}{2\sinh\eta\Delta} & -\frac{1}{2\sinh\eta\Delta} \\ \frac{e^{-\eta\Delta}}{2\sinh\eta\Delta} & -\frac{e^{\eta-\Delta}}{2\sinh\eta\Delta} & -\frac{1}{2\sinh\eta\Delta} & \frac{1}{2\sinh\eta\Delta} \end{pmatrix} \tag{A-12}$$

The normal forces are then computed from Eq. (2), Eq. (A-2) and Eq. (A-3):

$$N_1(X) = \frac{1}{2}(c_2 + c_3\eta(1+\chi)e^{-\eta X} - \eta c_4(1+\chi)e^{\eta X})A_1 - A_1\alpha_1\Delta_T \tag{A-13}$$

$$N_2(X) = \frac{1}{2}(c_2 - c_3\eta(1-\chi)e^{-\eta X} + \eta c_4(1-\chi)e^{\eta X})A_2 - A_2\alpha_2\Delta_T \tag{A-14}$$

The nodal normal forces are then deduced as function of the integration constants:

$$F_e + \begin{pmatrix} -A_1\alpha_1 \\ -A_2\alpha_2 \\ A_1\alpha_1 \\ A_2\alpha_2 \end{pmatrix}\Delta_T = N_e C \tag{A-15}$$

with:

$$N_e = \frac{1}{2}\begin{pmatrix} 0 & -A_1 & -\eta(1+\chi)A_1 & \eta(1+\chi)A_1 \\ 0 & -A_2 & \eta(1-\chi)A_2 & -\eta(1-\chi)A_2 \\ 0 & A_1 & \eta(1+\chi)e^{-\eta\Delta}A_1 & -\eta(1+\chi)e^{\eta\Delta}A_1 \\ 0 & A_2 & -\eta(1-\chi)e^{-\eta\Delta}A_2 & \eta(1-\chi)e^{\eta\Delta}A_2 \end{pmatrix} \tag{A-16}$$

In equation Eq. (A-15) the equivalent nodal force vector to the thermal load is appearing:

$$F_{th} = \begin{pmatrix} -A_1\alpha_1 \\ -A_2\alpha_2 \\ A_1\alpha_1 \\ A_2\alpha_2 \end{pmatrix} \Delta_T \qquad \text{(A-17)}$$

From Eq. (A-11) and Eq. (A-15), it comes:

$$F_e + F_{th} = N_e M_e^{-1} U_e \qquad \text{(A-18)}$$

The elementary stiffness matrix is finally computed from the matrix M_e and N_e:

$$K_{BBa} = N_e M_e^{-1} =$$

$$\frac{1}{1+\chi_A}\frac{A_2}{\Delta}\begin{pmatrix} \frac{\eta\Delta}{\tanh\eta\Delta} + \frac{1}{\chi_A} & 1 - \frac{\eta\Delta}{\tanh\eta\Delta} & -\frac{\eta\Delta}{\sinh\eta\Delta} - \frac{1}{\chi_A} & \frac{\eta\Delta}{\sinh\eta\Delta} - 1 \\ 1 - \frac{\eta\Delta}{\tanh\eta\Delta} & \frac{\eta\Delta}{\tanh\eta\Delta} + \chi_A & \frac{\eta\Delta}{\sinh\eta\Delta} - 1 & -\frac{\eta\Delta}{\sinh\eta\Delta} - \chi_A \\ -\frac{\eta\Delta}{\sinh\eta\Delta} - \frac{1}{\chi_A} & \frac{\eta\Delta}{\sinh\eta\Delta} - 1 & \frac{\eta\Delta}{\tanh\eta\Delta} + \frac{1}{\chi_A} & 1 - \frac{\eta\Delta}{\tanh\eta\Delta} \\ \frac{\eta\Delta}{\sinh\eta\Delta} - 1 & -\frac{\eta\Delta}{\sinh\eta\Delta} - \chi_A & 1 - \frac{\eta\Delta}{\tanh\eta\Delta} & \frac{\eta\Delta}{\tanh\eta\Delta} + \chi_A \end{pmatrix} \qquad \text{(A-19)}$$

The elementary stiffness matrix of the bar element, simulating the adherend j outside the overlap is:

$$K_{bar,j} = A_j \begin{pmatrix} 1 & -1 \\ -1 & 1 \end{pmatrix}, \ j = 1,2 \qquad \text{(A-20)}$$

Appendix B

This appendix provides the derivation of the constitutive equations of laminated beams used in the 1D-beam analysis, in the (X,Y_i,Z) reference local axis of the adherend, the height origin of which is taken on the neutral axis. The normal force and the bending moment are written such as:

$$N_i(X) = \int_{-h_i}^{+h_i} \sigma_i b dY_i = b \sum_{p_i=1}^{n_i} \int_{h_{p_i-1}}^{h_{p_i}} \sigma_i{}^{p_i} dY_i, \ i = 1,2 \qquad \text{(B-1)}$$

$$M_i(X) = \int_{-h_i}^{+h_i} -Y_i\sigma_i b dY_i = -b \sum_{p_i=1}^{n_i} \int_{h_{p_i-1}}^{h_{p_i}} \sigma_i{}^{p_i} Y_i dY_i, \ i = 1,2 \qquad \text{(B-2)}$$

where, in the adherend i n_i is the number of layers and h_{pi} is the *final* height of the p_i^{th} layer.

Moreover, the orthotopic behavior provides

$$\sigma_i{}^{p_i} = Q_i{}^{p_i}\big(\varepsilon_i{}^{p_i} - \alpha_i^{p_i}\Delta_T\big), \ i = 1,2 \qquad \text{(B-3)}$$

where, in the adherend I, $Q_i{}^{p_i}$ is the matrix of reduced stiffness in the $p_i{}^{th}$ layer.

As a result, the normal force and the bending moment are given by:

$$N_i(X) = b \sum_{p_i=1}^{n_i} \int_{h_{p_i-1}}^{h_{p_i}} Q_i{}^{p_i}\left(\varepsilon_i{}^{p_i} - \alpha_i^{p_i}\Delta_T\right)dY_i, \quad i = 1,2 \tag{B-4}$$

$$M_i(X) = -b \sum_{p_i=1}^{n_i} \int_{h_{p_i-1}}^{h_{p_i}} Q_i{}^{p_i}\left(\varepsilon_i{}^{p_i} - \alpha_i^{p_i}\Delta_T\right)Y_i dY_i \quad i = 1,2 \tag{B-5}$$

which finally leads to:

$$N_i(x) =$$

$$\sum_{p_i=1}^{n_i} Q_i{}^{p_i}\left[\int_{h_{p_i-1}}^{h_{p_i}} dy_i\right]\frac{du_i}{dx} - b \sum_{p_i=1}^{n_i} Q_i{}^{p_i}\left[\int_{h_{p_i-1}}^{h_{p_i}} y_i dy_i\right]\frac{d\theta_i}{dx} - b \sum_{p_i=1}^{n_i} Q_i{}^{p_i}\alpha_i^{p_i}\left[\int_{h_{p_i-1}}^{h_{p_i}} dy_i\right]\Delta_T$$

(B-6)

$$M_i(x) =$$

$$b \sum_{p_i=1}^{n_i} Q_i{}^{p_i}\left[\int_{h_{p_i-1}}^{h_{p_i}} y_i dy_i\right]\frac{du_i}{dx} + b \sum_{p_i=1}^{n_i} Q_i{}^{p_i}\left[\int_{h_{p_i-1}}^{h_{p_i}} y_i{}^2 dy_i\right]\frac{d\theta_i}{dx} +$$

$$\sum_{p_i=1}^{n_i} Q_i{}^{p_i}\alpha_i^{p_i}\left[\int_{h_{p_i-1}}^{h_{p_i}} y_i dy_i\right]\Delta_T \tag{B-7}$$

The parameters involving in the constitutive equations Eq. (31) to Eq. (33) are thus defined such as for i=1,2

$$A_i = b \sum_{p_i=1}^{n_i} Q_i{}^{p_i}\left(h_{p_i} - h_{p_i-1}\right) \tag{B-8}$$

$$B_i = \frac{b}{2}\sum_{p_i=1}^{n_i} Q_i{}^{p_i}\left(h_{p_i}{}^2 - h_{p_i-1}{}^2\right) \tag{B-9}$$

$$D_i = \frac{b}{3}\sum_{p_i=1}^{n_i} Q_i{}^{p_i}\left(h_{p_i}{}^3 - h_{p_i-1}{}^3\right) \tag{B-10}$$

$$N_i^{\bar{T}} = b \sum_{p_i=1}^{n_i} Q_i{}^{p_i}\alpha_i^{p_i}\left(h_{p_i} - h_{p_i-1}\right)\Delta_T \tag{B-11}$$

$$M_i^{\bar{T}} = \frac{b}{2}\sum_{p_i=1}^{n_i} Q_i{}^{p_i}\alpha_i^{p_i}\left(h_{p_i}{}^2 - h_{p_i-1}{}^2\right)\Delta_T \tag{B-12}$$

Appendix C

This appendix provides a brief description of the formulation of the beam element used in the 1D-beam analysis. Under the approximation of small bending angle, the local equilibrium equations of adherend $i=1,2$ outside the overlap are given by:

$$\frac{dN_i}{dX} = 0 \tag{C-1}$$

$$\frac{dV_i}{dX} = 0 \tag{C-2}$$

$$\frac{dM_i}{dX} + V_i - N_i\theta_i = 0 \tag{C-3}$$

It corresponds to those obtained along the overlap when the adhesive stresses vanish. But, the normal force is equal to F at any X. The system of six first order linear ODEs to be solved is then found under the following shape:

$$\frac{du_i}{dX} = \frac{D_i}{\Delta_i}N_1 + \frac{B_i}{\Delta_i}M_i \tag{C-4}$$

$$\frac{dv_i}{dX} = \theta_i \tag{C-5}$$

$$\frac{d\theta_i}{dX} = \frac{B_i}{\Delta_i}N_i + \frac{A_i}{\Delta_i}M_i \tag{C-6}$$

$$\frac{dN_i}{dX} = 0 \tag{C-7}$$

$$\frac{dV_i}{dX} = 0 \tag{C-8}$$

$$\frac{dM_i}{dX} = -V_i + F\theta_i \tag{C-9}$$

The resolution is performed using the exponential matrix as described in section 2.2.3.

Appendix D

In [39-40], a path to take into account for a linear variation of the shear stress in the adherend thickness following [28] in the formulation of MEs is described and reminded here. In the 1D-bar analysis, it is sufficient to modify the adhesive shear relative stiffness such as:

$$k_{II} = \frac{1}{1+\beta}\frac{G_a}{e_a} \tag{D-1}$$

with:

$$\beta = \frac{1}{3}\frac{G_a}{e_a}\left(\frac{e_1}{G_1} + \frac{e_2}{G_2}\right) \tag{D-2}$$

where G_1 (G_2) is the shear modulus of the adherend 1 (2).

In the 1D-beam analysis, the constitutive equations of adherends to consider are:

$$N_i = A_i \frac{du_i}{dx} - B_i \frac{d\theta_i}{dx} - C_i \frac{dT}{dx} - N_i^{\Delta T} \tag{D-3}$$

$$M_i = -B_i \frac{du_i}{dx} + D_i \frac{d\theta_i}{dx} + C'_i \frac{dT}{dx} + M_i^{\Delta T} \tag{D-4}$$

$$\theta_i = \frac{dv_i}{dx} \tag{D-5}$$

where, for i=1,2:

$$C_i = \frac{e_i B_i + (-1)^i D_i}{2e_i G_i} = \frac{1}{2}\left(\frac{B_i}{G_i} + (-1)^i \frac{D_i}{2h_i G_i}\right) \tag{D-6}$$

$$C'_i = \frac{e_i D_i + (-1)^i F_i}{2e_i G_i} = \frac{1}{2}\left(\frac{D_i}{G_i} + (-1)^i \frac{F_i}{2h_i G_i}\right) \tag{D-7}$$

$$F_i = \frac{b}{4}\sum_{p_i=1}^{n_i} Q_i^{p_i}\left(h_{p_i}^{\ 4} - h_{p_i-1}^{\ 4}\right) \tag{D-8}$$

Beside, to replace the Euler-Bernoulli beam model by the beam model, it is sufficient to replace the normality equation:

$$\frac{dv_i}{dX} = \theta_i \tag{D-9}$$

by:

$$V_i = H_i\left(\frac{dv_i}{dx} - \theta_i\right) \tag{D-10}$$

where H_i is the shear stiffness taken into account the shear correction factor.

References

1. Hart-Smith, LJ, 1982. Design methodology for bonded-bolted composite joints. Technical Report, AFWAL-TR-81-3154, Douglas Aircraft Company, Long Beach, California.

2. Kelly, G, 2006. Quasi-static strength and fatigue life of hybrid (bonded/bolted) composite single-lap joints. Compos. Struct., 72, 119-129.

3. da Silva, LFM, Öschner, A, Adams, RD (Editors), 2018. Handbook of Adhesion Technology (2 volumes), 2nd edition Springer, Heidelberg, Germany.

4. ASTM D5656-95. Standard Test Method for Thick-Adherend Metal Lap-Shear Joints for the Stress-strain Behavior of adhesives by Tension Loading. ASTM 1995.

5. Cognard, JY, Créac'hcadec, R, Sohier, L, Leguillon, D, 2010. Influence of adhesive thickness on the behaviour of bonded assemblies under shear loadings using a modified TAST fixture. Int. J. Adhes. Adhes., 30, 257-266.

6. Hart-Smith, LJ, 1973. Adhesive-bonded scarf and stepped-lap joints. Technical Report, NASA, CR112237, Douglas Aircraft Company, Long Beach, California.

7. Oterkus, E., Barut, A., Madenci, E., Smeltzer, S.S., Ambur, D.R., 2004. Nonlinear analysis of bonded composite joints, 45th AIAA/ASME/ASCE/AHS/ASC Structures, Structural Dynamics, and Materials Conference, 19-22 April 2004, Palm Springs, California.

8. Zhao, X, Adams, RD, da Silva, LFM, 2011a. Single lap joints with rounded adherend corners: Stress and strain analysis. J. Adhes. Sci. Technol., 25, 819-836.

9. Zhao, X, Adams, RD, da Silva, LFM, 2011b. Single lap joints with rounded adherend corners: Experimental results and strength prediction, J. Adhes. Sci. Technol., 25, 837-856.

10. Raphael, C, 1966. Variable-adhesive bonded joints. In: Proceedings of the Applied Polymer Symposium, 3, 99-108.

11. da Silva, LFM, Lopes, MJCQ, 2009. Joint strength optimization by the mixed-adhesive technique. . Int. J. Adhes. Adhes., 29(5), 509-514.

12. Breto, R, Chiminelli, A, Duvivier, E, Lizaranzu, M, Jiménez, MA, 2015. Finite Element Analysis of Functionally Graded Bond-Lines for Metal/Composite Joints. J. Adhesion, 91, 920-936.

13. Machado, J, Marques, E, da Silva, LFM, 2018. Influence of low and high temperature on mixed adhesive joints under quasi-static and impact conditions. Compos. Struct., 194, 68-79.

14. Durodola, JF, 2017. Functionally graded adhesive joints – A review and prospects. Int. J. Adhes. Adhes., 76, 83-89.

15. Kawasaki, S, Nakajima, G, Haraga, K, Sato, C, 2016. Functionally Graded Adhesive Joints Bonded by Honeymoon Adhesion Using Two Types of Second Generation Acrylic Adhesives of Two Components. J. Adhesion, 92(7-9), 517-534.

16. van Ingen, JW, Vlot, A, 1993. Stress analysis of adhesively bonded single lap joints. Report LR-740, Delft University of Technology. The Netherlands.

17. Tsaï, MY, Morton, J, 1994. An evaluation of analytical and numerical solutions to the single-lap joint. Int. J. Solids Struct., 31, 2537-2563.

18. da Silva, LFM, das Neves, PJC, Adams, RD, Spelt, JK, 2009. Analytical models of adhesively bonded joints-Part I: Literature survey. Int. J. Adhes. Adhes., 29, 319-330.

19. Carbas, RJC, da Silva, LFM, Madureira, ML, Critchlow, GW, 2014. Modelling of functionally graded adhesive joints. J. Adhesion, 90(8), 698-716.

20. Volkersen, O, 1938. Die Nietkraftverteilung in Zugbeanspruchten Nietverbindungen mit konstanten Laschenquerschnitten, Luftfahrforschung. 15(24), 41-47.

21. Stein, N, Weißgraeber, P, Becker, W, 2016. Stress solution for functionally graded adhesive joints. Int. J. Solids Struct., 97-98, 300-311.

22. Stein, N, Felger, J, Becker, W, 2017. Analytical models for functionally graded adhesive joints: A comparative study, Int. J. Adhes. Adhes., 76, 70-82.

23. Goland, M, Reissner, E, 1944. The stresses in cemented joints, J. Appl. Mech., 11, A17-A27.

24. Hart-Smith, LJ, 1973. Adhesive bonded single lap joints. NASA Technical Report, CR-112236, Douglas Aircraft Company, Long Beach, California.

25. Williams, JH, 1975. Stresses in adhesive between dissimilar adherends. J. Adhesion, 7, 97-107.

26. Bigwood, DA, Crocombe AD, 1989. Elastic analysis and engineering design formulae for bonded joints. Int. J. Adhes. Adhes., 9(4), 229-242.

27. Oplinger, DW, 1991. A Layered Beam Theory for Single-Lap Joints, Technical Report, US AMTL, MTL91-23.

28. Tsaï, MY, Oplinger, DW, Morton, J., 1998. Improved Theoretical Solutions for Adhesive Lap Joints Int. J. Solids Struct., 35(12), 1163-1185.

29. Högberg, JL, 2004. Mechanical behavior of single-layer adhesive joints − An Integrated approach. Licensing Graduate Thesis, Department of Applied Mechanics, Chalmers University of Technology, Sweden.

30. Nemes, O, Lachaud, F, 2009. Modeling of cylindrical adhesively bonded joints, J. Adhes. Sci. Technol., 23(10-11), 1383-1393.

31. Luo, Q, Tong, L, 2007. Fully-coupled nonlinear analysis of single lap adhesive joints. Int. J. Solids Struct., 44, 2349-2370.

32. Weißgraeber, P, Stein, N, Becker, W, 2014. A general sandwich-type model for adhesive joints with composite adherends. Int. J. Adhes. Adhes., 55, 56–63.

33. Talmon de l'Armée, A, Stein, N, Becker, W, 2016. Bending moment calculation for single lap joints. Int. J. Solids Struct., 66, 41−52.

34. Stapleton, SE, Weimer, J, Spengler, J, 2017. Design of functionally graded joints using a polyurethane-based adhesive with varying amounts of acrylate, Int. J. Adhes. Adhes., 76, 38-46.

35. Stapleton, SE, 2012. The analysis of adhesively bonded advanced composite joints using joint finite elements. PhD thesis, University of Michigan. Michigan.

36. Paroissien, E, 2006. Contribution aux Assemblages Hybrides (Boulonnés/Collés) − Application aux Jonctions Aéronautiques. PhD Dissertation (in French), Université de Toulouse III.

37. Paroissien, E, Sartor, M, Huet, J, 2007. Hybrid (bolted/bonded) joints applied to aeronautic parts: Analytical one-dimensional models of a single-lap joint. In: Advanced in Integrated Design and Manufacturing in Mechanical Engineering II. S Tichkiewitch, M Tollenaere, and P Ray (Eds.), 95-110, Springer, Dordrecht, The Netherlands.

38. Paroissien, E, Sartor, M, Huet, J, Lachaud, F, 2007. Analytical two-dimensional model of a hybrid (bolted/bonded) single-lap joint, J. Aircraft, 44, 573-582.

39. Paroissien, E, Lachaud, F, Jacobs T, 2013. A simplified stress analysis of bonded joints using macro-elements. In: Advances in Modeling and Design of Adhesively Bonded Systems, Kumar S. and Mittal K.L. (Eds), 93-146, Wiley-Scrivener, Beverly, Massachusetts.

40. Paroissien, E, Gaubert, F, Da Veiga, A, Lachaud, F, 2013. Elasto-Plastic Analysis of Bonded Joints with Macro-Elements. J. Adhes. Sci. Technol., 27(13), 1464-1498.

41. Lélias, G, Paroissien, E, Lachaud, F, Morlier, J, Schwartz, S, Gavoille, C, 2015. An extended semi-analytical formulation for fast and reliable mode I/II stress analysis of adhesively bonded joints. Int. J. Solids Struct., 62, 18-38.

42. Lélias, G, 2016. Mechanical behavior of adhesively bonded joints: Modeling, simulation and experimental characterization. PhD Thesis, University of Toulouse 3, Toulouse, France.

43. Paroissien, E, Lachaud, F, Da Veiga, A, Barrière, P, 2017. Simplified Stress Analysis of Hybrid (Bolted/Bonded) Joints. Int. J. Adhes. Adhes., 77, 183-197.

44. Hart-Smith, LJ, 1973c. Adhesive-Bonded Double-Lap Joints. NASA Technical Report, CR112235, Douglas Aircraft Company, Long Beach, California.

45. Zeyfang, R, 1971. Stresses and strains in a plate bonded to a substrate: Semiconductor devices. Solid State Electron., 14, 1035-1039.

46. Chen, WT, Nelson, CW, 1979. Thermal stresses in Bonded Joints. IBM J. R&D, 23(2), 179-188.

47. Suhir, E, 1986. Stresses in bi-material thermostat. J. Appl. Mech., 53, 657-660.

48. Marques, EAS, da Silva, LFM, Banea, MD, Carbas, R, 2015. Adhesive joints for low and high temperature use: An overview. J. Adhesion, 91, 556–585.